

Organization of Paramagnetic and Nonmagnetic Colloidal Particles in Ferrofluid

Von der Universität Bayreuth
zur Erlangung des Grades eines
Doktors der Naturwissenschaften (Dr. rer. nat.)
genehmigte Abhandlung

von

Ayan Ray

geboren am 27. Nov. 1983 in Kalkutta/Indien

1. Gutachter: Prof. Dr. Th .M. Fischer
2. Gutachter: Prof. Dr. W. Köhler

Tag der Einreichung: 17.04.2012

Tag des Kolloquiums: 21.06.2012

Dedicated to my beloved father Prof. K. K. Ray (baba) and mother Mrs. S.
Ray (maa)

Acknowledgement

I would like to thank and express my sincere gratitude to Professor Dr. Thomas Fischer for his kind and caring guidance, and constant support during my doctoral study at the University of Bayreuth, Germany. I would also like to thank him specially for introducing me to the new world of "Dynamics of Soft Matter" in physics. This thesis work would not have been possible without his scientific advice, personal guidance and understanding. Professor Thomas is more like a friend than a supervisor to me.

I take this opportunity to thank all my group members Uli Langer, Nebojsa Casic, Tobias Gehring, Saeedeh Aliaskarisohi and Christiane Jungnickel who helped me with their scientific and technical knowledge apart from their personal help whenever required. Getting such a galaxy of friendly colleagues in one place is hard to find now-a-days. Altogether it was a small family with precious sweet memories.

I would also like to thank all the members of Experimental Physics V for their constant support whether technical or scientific discussions.

At this point I would like to thank specially Mrs. Carmen Kerling for helping me in the IT sector, Mr. Klaus Oetter for his assistance in manufacturing of different machined components at Bayreuth and our group secretary Mrs. Christine Linser helping me with the official, administrative works and her

valuable suggestions towards societal relations. After all, a cup of coffee is an unequalled medium to restore and keep up spirits.

Taking this opportunity I would like to thank the Welcome Center of the University of Bayreuth and personally Dr. Cornelia Nicodemus for her help and guidance throughout my stay at Bayreuth.

I take this opportunity to express my heartfelt thanks to my contemporary research colleagues and friends - Sonal Di, Swastik Da and boudi (Aditi), Dr. Himadri da and boudi (Dolon), Imran, Somnath, Pratap, Andy, Moritz, Christian and Marrion and many others of the University of Bayreuth for their kind help at required moments and for making my stay at Bayreuth a happy and memorable one.

All along this work my beloved friend Sayanti has remained as a source of inspiration, and assurance; I express my heartfelt deep gratitude to Sayanti for her love, patience and mental company at all moments to make this achievement a reality.

Finally, I would like to thank my parents, for always being with me throughout my studies and for their endless love and support. Their love and motivation was one of the key to the success of this dissertation.

Ayan Ray

Contents

1	Introduction	1
1.1	Introduction	1
1.2	Colloidal flower	5
1.3	Transition strength	6
1.4	Colloidal phases	9
2	Materials and Method	13
2.1	Materials	13
2.1.1	Ferrofluid	13
2.1.2	Magnetic Field	15
2.1.3	Optical Microscopy	15
2.2	Method	16
2.2.1	Dynamics of self-assembly of flower-shaped magnetic colloidal clusters	16
2.2.2	The transition strength from solid to liquid colloidal dipolar clusters in precessing magnetic fields	17
2.2.3	Magnetic field controlled composite paramagnetic-diamagnetic colloidal phases	20

3	Colloidal flower	23
4	Transition strength	31
5	Colloidal phases	41
6	Summary	65

List of Figures

- 1.1 a) schematic representation of colloidal flower-shaped clusters [7] formed in a perpendicular field H_z . The center particle is a paramagnetic particle, which is the core of the flower and the particles around the core are the diamagnetic particles that are referred as petals of the flower. b) represents X, Y and Z are the coordinate axis with H_x , H_y and H_z are the external magnetic field respectively. 6
- 1.2 a)Schematic representation of the behaviour of super-paramagnetic and nonmagnetic particles in an applied magnetic field when immersed in a thin film of ferrofluid; Figure 2a indicates that the direction of the applied magnetic field is in the z direction. Figure 2b shows a mixture of nonmagnetic and super-paramagnetic particles immersed in thin film of ferrofluid between two glass cover slips under the influence of the magnetic field. Figure 2c reveals the alignment of dipole moment of ferrofluid and Figure 2d shows the effective magnetic moment of the magnetic and nonmagnetic particles under an external applied magnetic field. It can be noted that Figure 2c and Figure 2d can combine to form Figure 2b. Here represent χ the susceptibility factor. . . . 7

1.3	<p>a) schematic representation of diamagnetic cluster formed in a rotating magnetic field H_{\parallel} in x-y plane. A core to petal size ratio is chosen to form the colloidal cluster. b) represents X, Y and Z are the coordinate axis with H_x, H_y and H_z are the external magnetic field with H_{\parallel} being the in plane rotating effective magnetic field and being the precession angle. Ω is the external applied frequency.</p>	9
1.4	<p>Schematic representation of magic angle.</p>	10
1.5	<p>Schematic presentation of the behaviour of nonmagnetic particles under a rotating magnetic field when immersed in a thin film of ferrofluid. Figure 5a indicates the direction of the applied magnetic field in the x-y plane. Figure 5b shows two different sizes of nonmagnetic particles immersed in thin film of ferrofluid between two glass coverslips under the influence of the rotating magnetic field. Figure 5c reveals the alignment of dipole moment of ferrofluid and Figure 4d shows the effective magnetic moment of nonmagnetic particles under an external applied rotating magnetic field, assuming the effect of ferrofluid to be negligible. It can be observed that Figure 5c and Figure 5d can combine to form figure 5b.</p>	11
1.6	<p>Schematic representation of the external magnetic field applied $\vec{H}(t) = \hat{H} \cos \vartheta_{ext} \vec{e}_z + \hat{H} \sin \vartheta_{ext} (\vec{e}_x \sin \Omega t + \vec{e}_y \sin 2\Omega t)$. $H(t)$ is the total external magnetic field strength applied to the sample. Where x,y and z are the coordinate axes.</p>	12

2.1	a) schematic representation of sample on top of solenoid and b) H_z being the external static magnetic field in the z direction. Here x, y and z are the coordinate axes.	17
2.2	a) Schematic representation of arrangements of five sets of solenoid coils and b) the combined rotating magnetic field $H_{ }$ and the perpendicular field H_{\perp} with ω being the angular frequency and the precession angle	19
2.3	a) schematic representation of the arrangement of solenoid coils and b) time dependent magnetic field produced by the five sets of solenoid coils similar to Lissajou curve.	21

Abstract

In this thesis, I have studied magnetic dipolar interactions between paramagnetic and nonmagnetic colloidal particles immersed in a magnetic fluid under the influence of an external time dependent magnetic field. These interactions play an important role in colloidal self-assembly. As a result, of these interactions different forms of anisotropic superstructures evolve in 2-Dimension and 3-Dimension during the self-assembly process. The time dependent external magnetic field is an important controlling parameter for the self-assembly process. The interactions leads to a specific equilibrium positions of the paramagnetic and nonmagnetic particles with specific orientations of the magnetic moments.

Three different colloidal systems immersed in ferrofluid with external time dependent magnetic field have been investigated. In each of them the effect of inter dipolar interactions on the particles is discussed. Three systems are arranged and discussed in three separate chapters. In chapter 3, an attempt has been made to study the diffusion of particles in a colloidal flower system and compare the diffusion of the petals of the flower with other single file diffusion in 1-dimension. Beside the long-range interactions, in chapter 4, we have studied the strength of the systems and order of phase transition taking place due to core size effects of self-assembled flower shaped magnetic colloidal clusters and diamagnetic clusters in a precessing magnetic field. In chapter 5, different anisotropic assemblies and colloidal phases are studies as a function of the composition mixture of paramagnetic and diamagnetic particles in an external time dependent magnetic field.

self-assembly, precessing magnetic field, ferrofluid, paramagnetic and non-magnetic particles, diamagnets

Zusammenfassung

In dieser Promotion habe ich magnetische Dipolwechselwirkungen zwischen paramagnetischen und nichtmagnetischen kolloidalen Partikeln in einer magnetischen Flüssigkeit unter dem Einfluß eines externen zeitabhängigen Magnetfeldes studiert. Diese Wechselwirkungen spielen eine wichtige Rolle bei der kolloidalen Selbstorganisation. Als Ergebnis dieser Wechselwirkungen erscheinen verschiedene Formen von zwei- und dreidimensionalen anisotropen Superstrukturen während des Selbstorganisationsprozesses. Das zeitabhängige externe magnetische Feld ist ein wichtiger Kontrollparameter für den Selbstorganisationsprozeß. Die Wechselwirkung führt zu spezifischen Gleichgewichtspositionen der paramagnetischen und der nichtmagnetischen Partikel mit einer spezifischen Orientierung der magnetischen Momente.

Drei verschiedene kolloidale Systeme in Ferrofluid mit externem zeitabhängigem Magnetfeld wurden untersucht. In jedem von Ihnen wird der Effekt von interpolaren Wechselwirkungen auf die Partikel diskutiert. Drei Systeme sind in drei einzelnen Kapiteln angeordnet und werden dort diskutiert. In Kapitel 3 wurde der Versuch gemacht die Diffusion von Partikeln in einer „kolloidalen Blume“ zu studieren und die Diffusion der Blütenblätter mit anderen single file Diffusionssystemen in einer Dimension zu vergleichen. Neben den langreichweitigen Wechselwirkungen haben wir in Kapitel 4 den Einfluß der Größe des Kerns der kolloidalen Blumen und Cluster auf die Stärke des Phasenübergangs erster Ordnung von einem Cluster zu einer Flüssigkeit untersucht. In Kapitel 5 werden verschiedene anisotropische Ansammlungen und kolloidale Phasen in Abhängigkeit der Zusammensetzung der Mischung von paramagnetischen

und diamagnetischen Partikeln in einem externen zeitabhängigen Magnetfeld studiert.

Selbstorganisation, präzedierendes Magnetfeld, Ferrofluid, paramagnetische und unmagnetische Partikel, Diamagnete

Chapter 1

Introduction

1.1 Introduction

The structure and dynamics of colloids is an important scientific problem with profound implications in medical-, health care-, pharmaceutical -, oil recovery- and coating applications [6]. Colloids are a metastable ensemble of nanoscopic to micron-sized particles immersed in to a carrier fluid that are stabilized against aggregation via short-range (nanometer range) interactions.

The current thesis deals with colloids that beside the short-range interactions interact also via long-range magnetic dipole interactions. The questions addressed in this thesis are a) how static long-range dipolar interactions might affect the dynamics of the colloids and b) how dynamic dipolar interactions caused by time dependent external magnetic fields might affect the statics and dynamics of the colloids.

Dipolar interactions are long-range interactions because the energy of an ensemble of aligned dipoles is super-extensive, i.e. the dipole energy per unit volume grows logarithmically with the size of the sample. In order to render the

dipolar energy of a sample extensive dipolar interactions tend to destroy the alignment with superstructures of dipoles that point into different directions in different regions of the sample. Different dipolar colloidal particles therefore communicate with each other over large distances, while ordinary colloidal particles only interact when coming close. In chapter 3, we investigate the difference in diffusion of colloidal particles this long-range interaction causes in a single file of colloids that are not allowed to pass each other. For short-range interacting colloids, the single file diffusion is characterized by a delayed hard-core interaction. The colloids first have to freely diffuse toward a neighbour before they encounter the repulsive barrier imposed by the neighbour. In a single file diffusion system, such delay becomes apparent in the velocity autocorrelation function of the particles. A free diffusion positive correlated peak of the correlation function at short times is followed by an anti-correlated minimum at longer times. The effective diffusion constant over longer times is the integral over the velocity autocorrelation function and vanishes because the positive and negative regions in the correlation function cancel each other. As a result, the long time diffusive behaviour is subdiffusive. It is clear that colloidal particle interacting via long-range dipolar interactions feel the presence of the other particle immediately and therefore lack the delay for the single file diffusing [2] hard-core particles. One of the questions addressed in this thesis is therefore how do long-range dipolar interactions alter the hard-core single file diffusion.

Dipolar interactions are not only interesting because of their long range. They also have a very interesting angular dependence. The sign of the interaction depends on the angles both magnetic dipole moments enclose with the separation vector between both dipoles as well as on the angle between the

two dipole moments. This angular dependence is such that the interaction when averaged over all separation directions exactly vanishes. The trace of the dipolar interaction tensor vanishes. Attractive separation directions cancel repulsive interaction directions. For this reason, structures assembled via dipole interactions can never be isotropic. They are always anisotropic. If we apply external magnetic fields to the sample that vary in direction on a time scale too fast for the individual particles to rearrange into the corresponding instantaneous equilibrium structure we can eliminate all dipolar interactions when scanning over attractive and repulsive directions just in a way such that attraction and repulsion cancel each other. The simplest way of averaging away dipolar interactions is by spinning at the magic angle, a technique extensively used in chemistry for the narrowing of NMR peaks. Here we apply precessing magnetic fields to an ensemble of magnetic colloids and use the precession angle as a control parameter of the self-assembled structure of the colloids. The dipolar interaction between particles switches sign when the precession angle passes the magic angle. As a result a structural rearrangement of the particles is caused and we might investigate the order of the structural phase transition happening in the system. The question addressed in chapter 4 is hence how the dynamics of structures caused by time dependent precessing external fields close to the magic angle reveal the order of the structural phase transition.

Our magnetically interacting colloids are paramagnetic colloids consisting of a polystyrene bead filled with grains of magnetite. Their dipole moment point into the direction of the local magnetic field with a magnitude that is proportional to the strength of the local magnetic field. In most of the applications studied in this thesis, depolarization fields of the particles are weak and the local field is dominated by the direction of the external field. In such

situation, all paramagnetic beads have magnetic moments that point into the same direction. We can enrich the structure of the assembly [5] by incorporating diamagnetic particles. Such diamagnets react to an external field with a magnetic moment anti-parallel to the external field. Since diamagnetic susceptibilities of most materials at room temperature are small, we must use a trick to obtain effective diamagnets. This trick consists of immersing nonmagnetic colloids into a ferrofluid. When using a ferrofluid with susceptibility between the zero susceptibility of the non-magnetic colloids and the susceptibility of the paramagnetic colloids the paramagnetic colloids still act as paramagnets while the non-magnetic beads act effectively as diamagnetic particles in the background of the ferrofluid. Such effective diamagnets run under the name magnetic holes. In chapter 5, we expose a mixture of paramagnets and magnetic holes [1] [3] to time dependent external fields to self assemble the mixture into various structures. The question addressed in this chapter is which type of anisotropic structures of the mixed system may be assembled when using various forms of external magnetic field modulations.

To answer these questions I have arranged the thesis into the following structure: chapter 1 includes a brief introduction to the thesis with motivation as a subsection. Experimental details have been provided in the subsection titled methodology with the materials parameter of chapter 2. Chapter 3, chapter 4, and chapter 5 are the attached published manuscripts with the results and conclusion. Finally, chapter 6 includes the summary.

1.2 Dynamics of self-assembly of flower-shaped magnetic colloidal clusters

In chapter 3, we were interested to study the effects of dynamic interactions of paramagnetic and nonmagnetic particles in a 1-dimensional system. We observed single file diffusion present in our system. Single file diffusion refers to the 1-dimensional motion of interacting particles in pores, which are so narrow that the mutual passage of such particles is excluded. Since the sequence of particles in such a situation remains unaffected over time t , leads to deviation from normal diffusion. Such a single file diffusion of colloids in 1-dimensional have already been reported [C. Lutz et al, 2004]. Where the colloidal particles were trapped by a scanning laser beam to a circular optical trap.

Our system consists of paramagnetic and nonmagnetic particles immersed in ferrofluid under static magnetic field (magnetic field strength $\vec{H}(t) = \hat{H}\vec{e}_z$, z-direction), sandwiched between two glass coverslips. Under such conditions flower shaped magnetic colloids are formed, where the paramagnetic particle is at the center i.e. the core of the flower and the nonmagnetic particles are at the equator, the petals, shown in Figure(1.1). External magnetic field induces magnetic moments in the particles that interacts via the dipole dipole interaction. Due to the presence of static magnetic field in the system of magnetic and nonmagnetic particles immersed in ferrofluid (chapter 3), the effective dipoles i.e. the magnetic dipole minus the ferrofluid background of the two sorts of particles point into opposite directions Figure(1.2). Hence, in presence of static magnetic field the nonmagnetic particles immersed in ferrofluid behaves as diamagnets and the paramagnets behaves still as paramagnets. These diamagnets are attracted towards the core (paramagnet) to

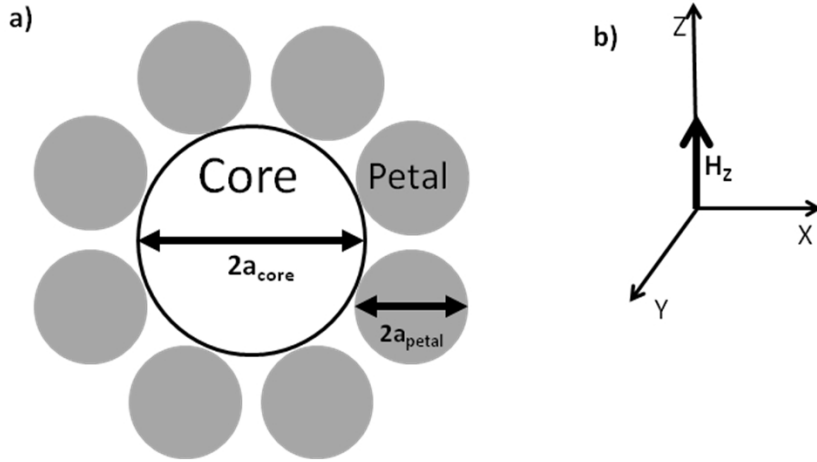


Figure 1.1: a) schematic representation of colloidal flower-shaped clusters [7] formed in a perpendicular field H_z . The center particle is a paramagnetic particle, which is the core of the flower and the particles around the core are the diamagnetic particles that are referred as petals of the flower. b) represents X, Y and Z are the coordinate axis with H_x , H_y and H_z are the external magnetic field respectively.

form a circular channel. Around the core the diamagnets have a repulsive force between each other and interact by soft-core interactions. The motions of these interacting particles (diamagnets) in the circular array made us motivated to study and characterize the single file diffusion in the self-assembled flower-shaped magnetic colloidal clusters.

1.3 The transition strength from solid to liquid colloidal dipolar cluster in precessing magnetic fields

Due to the presence of hard-core and dipolar interactions present in the magnetic colloidal flower system we can study the influence of long range interactions on to the single file diffusion chapter 3. Long-range interactions also

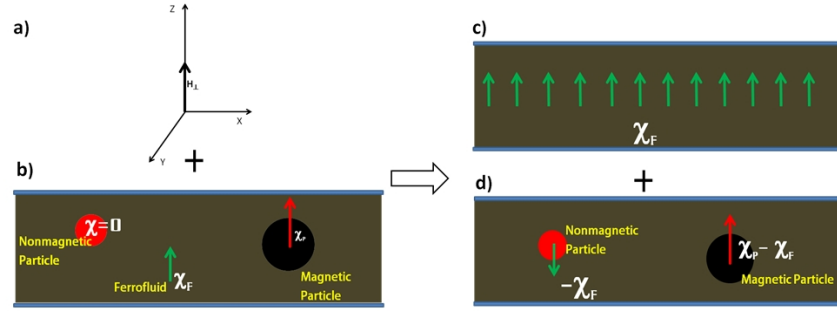


Figure 1.2: a) Schematic representation of the behaviour of super-paramagnetic and nonmagnetic particles in an applied magnetic field when immersed in a thin film of ferrofluid; Figure 2a indicates that the direction of the applied magnetic field is in the z direction. Figure 2b shows a mixture of nonmagnetic and super-paramagnetic particles immersed in thin film of ferrofluid between two glass cover slips under the influence of the magnetic field. Figure 2c reveals the alignment of dipole moment of ferrofluid and Figure 2d shows the effective magnetic moment of the magnetic and nonmagnetic particles under an external applied magnetic field. It can be noted that Figure 2c and Figure 2d can combine to form Figure 2b. Here represent χ the susceptibility factor.

play an essential role for phase transitions between differently ordered phases. A first-order phase transitions exhibit a discontinuous change in the order parameter. The change of one phase to other occurs via a coexistence of the two phases. The area of the hysteresis measures the dissipated energy when traversing the coexistence region back and forth. Whereas a second order phase transition is a transition where the order parameter changes continuously at the transition. Second order transitions are associated with critical behavior of response functions as a function of the control parameter while first order transitions exhibit no critical behavior.

The formation and rupture of flower-shaped magnetic colloidal clusters can be considered as a finite size phase transitions. It was a question of interest, is the change in the hysteresis could reveal the strength and order of the phase transitions in the system. The formation and rupture of the flower-

shaped magnetic colloidal clusters and diamagnetic clusters takes place with the change in the precession angle, the control parameter. A hysteresis loop is observed when tuned the precession angle, from low to high and vice versa. Whether the study of the width of the hysteresis could reveal the order of the system? Besides, is it possible to define the order and strength by the measuring the response function, the angular velocity of the particles as a function of change in the precession angle?

These flower-shaped magnetic colloidal clusters were formed from paramagnetic and nonmagnetic particles immersed in diluted ferrofluid under a static magnetic field in the z-direction and sandwiched between two glass coverslips (Figure (1.1)). Whereas the diamagnetic colloidal clusters were formed from nonmagnetic particles immersed in concentrated ferrofluid under a rotating field Figure(1.3) and sandwiched between two glass coverslips. The magnetic field strength being $\vec{H}(t) = \hat{H}(\vec{e}_x \sin \Omega t + \vec{e}_y \cos \Omega t)$, with Ω being the angular frequency in x-y plane. The flower-shaped magnetic colloidal were stable at low angles and nearby the magic angle these structures were unstable whereas, the diamagnetic clusters were stable at high angles and their stability decreased reaching towards the magic angle. Here the magic angle ϑ_{magic} is the defined as a unique angle, which is approximately 54.73° . It is the root of a second-order Legendre polynomial $P_2(\cos \theta) = 0$ and interactions depending on this second-order Legendre polynomial vanishes at this angle. Mathematically $\vartheta_{\text{magic}} = \theta_m = \arctan \sqrt{2} \approx 54.73^\circ$, Figure(1.4). As external magnetic field induces magnetic moments in the particles and they interact via dipole dipole interaction. The effective dipoles (diamagnetic cluster formation) i.e. the magnetic dipole minus the ferrofluid background of the two sorts of particles point into same directions (x-y plane), shown in Figure(1.5). Similarly, in

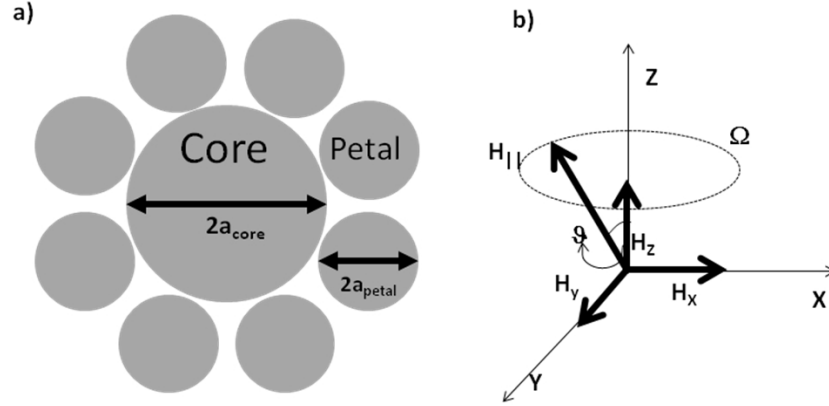


Figure 1.3: a) schematic representation of diamagnetic cluster formed in a rotating magnetic field H_{\parallel} in x-y plane. A core to petal size ratio is chosen to form the colloidal cluster. b) represents X, Y and Z are the coordinate axis with H_x , H_y and H_z are the external magnetic field with H_{\parallel} being the in plane rotating effective magnetic field and being the precession angle. Ω is the external applied frequency.

both the systems of colloidal flower and diamagnetic cluster due to the presence of external magnetic field the particles interact via dipole dipole interaction.

1.4 Magnetic field controlled composite paramagnetic-diamagnetic colloidal phases

Neutralization of opposite charge is one of the major concepts in ordinary matter where two opposite charges cancel each other. The interactions taking place between these opposite charges is isotropic and is independent of direction. This charge neutralization is the key towards the organizations of matter on the atomic and molecular scale leading to self-assembly. It is spontaneous breaking of rotational symmetry [4] and the quantization of angular momentum that produces crystalline structures with forming direct bonds in atoms and molecules. Whereas, neutralization process is different in case of mesoscopic

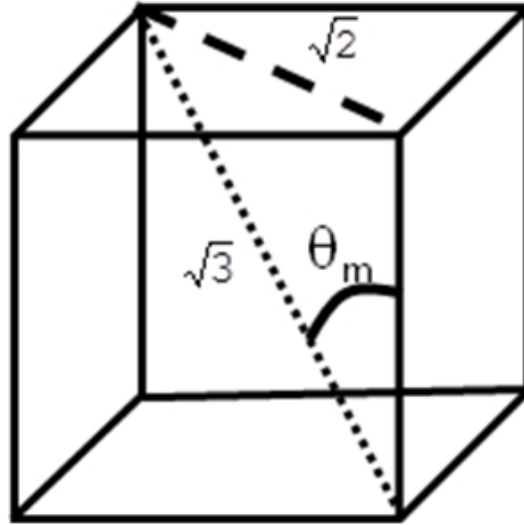


Figure 1.4: Schematic representation of magic angle.

sized particles due to the absence of the quantum phenomena and angular momentum being a continuous quantity. In a colloidal system the direct bond formation does not work. Steric interactions are the means to spontaneously break the rotation symmetry to form colloidal crystal for isotropic structures. Direct bond in colloidal system are only possible using intrinsically anisotropic colloidal particles e.g. Janus or ellipsoid particles.

One of the other possibilities to use the magnetic or electric dipole moment using an external field. In case for a mixture of paramagnetic and nonmagnetic particles immersed in a magnetic fluid under magnetic field. The effective dipole moment induced due to the same external magnetic field results in pointing the dipoles into opposite direction for paramagnetic and nonmagnetic particles. The induced magnetic moment neutralizes each other similarly like the charge neutralization, forming rich variety of anisotropic self-assembled structures. An attempt has been made to study this charge neutralization of magnetic moments in an external magnetic field resulting in forming different anisotropic structures.

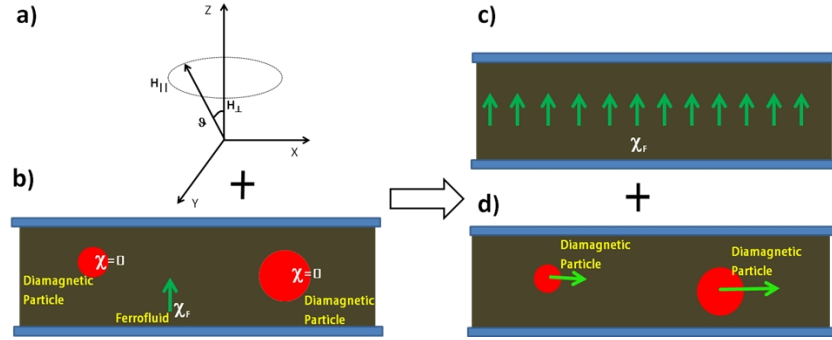


Figure 1.5: Schematic presentation of the behaviour of nonmagnetic particles under a rotating magnetic field when immersed in a thin film of ferrofluid. Figure 5a indicates the direction of the applied magnetic field in the x-y plane. Figure 5b shows two different sizes of nonmagnetic particles immersed in thin film of ferrofluid between two glass coverslips under the influence of the rotating magnetic field. Figure 5c reveals the alignment of dipole moment of ferrofluid and Figure 4d shows the effective magnetic moment of nonmagnetic particles under an external applied rotating magnetic field, assuming the effect of ferrofluid to be negligible. It can be observed that Figure 5c and Figure 5d can combine to form figure 5b.

Our system consists of paramagnetic and nonmagnetic particles immersed in ferrofluid under a magnetic field $\vec{H}(t) = \hat{H} \cos \vartheta_{ext} \vec{e}_z + \hat{H} \sin \vartheta_{ext} (\vec{e}_x \sin \Omega t + \vec{e}_y \sin 2\Omega t)$ as shown in Figure (1.5), sandwiched between two glass coverslips. We use magnetic field with three different frequencies with zero-frequency, Ω and $2 - \Omega$ frequency along different axes. This magnetic field was applied to the particles such that there is no torque.

Dipolar interactions are anisotropic and differ in sign for interactions between similar (paramagnetic or diamagnetic) particles and opposite (paramagnetic and diamagnetic) particles. The composite structure of a mixture of diamagnetic s and paramagnets is therefore expected to exhibit a rich variety of structures. These structures will be explored in chapter 5.

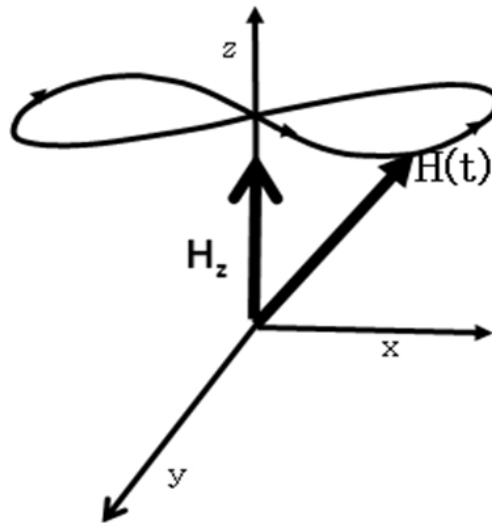


Figure 1.6: Schematic representation of the external magnetic field applied $\vec{H}(t) = \hat{H} \cos \vartheta_{ext} \vec{e}_z + \hat{H} \sin \vartheta_{ext} (\vec{e}_x \sin \Omega t + \vec{e}_y \sin 2\Omega t)$. $H(t)$ is the total external magnetic field strength applied to the sample. Where x, y and z are the coordinate axes.

Chapter 2

Materials and Method

2.1 Materials

2.1.1 Ferrofluid

Ferrofluid is a complex fluid, which has magnetic properties like solid while being a fluid in its physical state. The ferrofluids contain tiny magnetic materials of the order 10 – 12 nm in size in a liquid medium. These nanometer-sized particles are coated with a stabilizing dispersing agent, which prevents particle agglomeration even under an applied strong magnetic field gradient. Depending on the medium, these ferrofluids can be classified either as (a) oil based or (b) water based. For the current experiments, water based ferrofluids were procured from Ferrotec Ferrosound. Ferrofluid EMG 705 and EMG 707 were two water-based ferrofluids used for the present experiments. The EMG 705 has a saturation magnetization at 22 mT with magnetic susceptibility of 4.04 (SI units) whereas the EMG 707 has 11 mT with susceptibility of 1.51 (SI Units) [Ferrotec Ferrosound USA]. Super-paramagnetic beads Spheri-

cal super-paramagnetic beads (M-270 and MyOne) have been purchased from Dynal Invitrogen (Invitrogen Dynal Oslo, Norway). These procured beads were highly monodisperse and had a mean diameter of either $2.8\ \mu\text{m}$ with concentration of 2.8×10^9 beads/ml or $1.0\ \mu\text{m}$ with concentration of 10 mg/l. Colloids made of these particles are paramagnetic in nature and have a core shell structure. The core of the particles is filled with nanometer-sized grains of magnetite that is surrounded by a polymer shell. The surface of the colloids used here is functionalized with carboxylate groups, which dissociate in water and cause a negative surface charge on the particles. On a nanometer scale, these particles repel each other, which prevent the aggregation of the beads. The magnetite core renders the particles paramagnetic in an external field in proportion to the applied magnetic field. Therefore, the individual particles interact on a large scale via magnetic dipole-dipole interactions. Moreover, the particles have a large surface area, high capacity, efficient magnetic pull and a low sedimentation rate during incubation [Invitrogen, MyOne and M-270]. The hydrophilic nature of the particles assists in preventing particle agglomeration or particle sticking to the surfaces Polystyrene Beads Fluorescent spherical polystyrene dyed microparticles (beads) have been procured from three companies namely Fluoro-Max (ThermoFischer Scientific), Duke Scientific (Thermo Scientific Palo Alto, CA) and Spherotec (Lake Forest Illionis). The differently coloured micro particles were visible whether it is polarization or fluorescence microscopic technique employed for their examinations. The mean diameters of the mono-dispersed particles ranged from $0.5\ \mu\text{m}$ to $9.9\ \mu\text{m}$. The concentration of these particles was either 1% solids/weight or 1% weight/volume depending on the source of procurement. The different labeling of fluorescent groups helped not only in distinguishing each system from the other but also

assisted to identify nature of the specific particles under fluorescence microscope. These dyed fluorescent micro-particles were marginally less hydrophilic in nature than the Dynal super-paramagnetic beads; the problems related to particle agglomeration and sticking to the surface were avoided by using a mechanical shaker (IKA MS 3 basic, GmbH).

2.1.2 Magnetic Field

External magnetic field was applied using the help of different kinds of laboratory-fabricated solenoids machined at University of Bayreuth. Some of these solenoids had soft iron core, Mu-metal core or simply air core depending on the experimental requirements. The nature of the core was selected according to the requirement for maintaining varied intensity and uniformity of magnetic field on the samples. The amplitude / intensity of the magnetic field on the sample were varied by changing the current in the solenoids. The magnetic field produced by the solenoids was recorded using a Gauss meter (Lakeshore). Temperature at the solenoids was examined frequently by an infrared temperature sensor, which was however maintained at the ambient temperature. Water-cooled solenoids were also incorporated in the experiments wherever necessary to cool down the solenoids and avoid burning.

2.1.3 Optical Microscopy

The assembly process was observed under a Fluorescence Microscope (purchased from LEICA DM 5000 B) in a reflection mode. Dual fluorescence band gap filters of green and red were used to observe micro-particles of two differently dyed fluorescence particles simultaneously. In addition, a plane Polarizer

filter was used to observe the Dynal beads, which were non-fluorescent. In addition, Digital fast black and white camera from Leica with an air c-mount was used to record the live movements. Most of the clippings stored by the camera were recorded using ~ 27 frames per second.

2.2 Method

2.2.1 Dynamics of self-assembly of flower-shaped magnetic colloidal clusters

Sample Preparation: A mixture of paramagnetic particles (diameter $2a = 2.8 \mu\text{m}$) with nonmagnetic fluorescent (red) polystyrene particles (diameter $2a = 1.0 \mu\text{m}$) immersed in 20% diluted ferrofluid EMG 705 was prepared in controlled proportions (paramagnetic 1 : nonmagnetic 4 by volume). This mixture was vigorously shaken to form a homogenous mixture. Using a pipette a small amount $0.5 \mu\text{l}$ of this mixture was placed at the center between two pre-cleaned glass cover slips. Extra care was taken while placing the top glass cover slip such that no air bubble exists to reduce drift. **External Field and Optical Microscopy:** The sample was placed on top of a solenoid, shown in Figure (2.1). An electric current of 0.43 Ampere was supplied to produce a static magnetic field of 10.0 mT in the z-direction.

This sample was observed under fluorescence microscope in a reflecting mode. Red fluorescence filter was used to observe the red fluorescence particles whereas the Polarization filter was used to observe the non-fluorescence paramagnetic particles. **Observations and recording:** When observed with the red filter fluorescence particles of the colloidal flowers i.e the petals were observed.

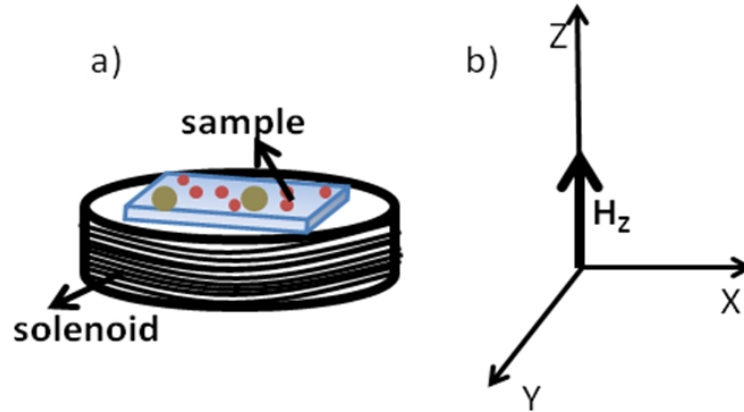


Figure 2.1: a) schematic representation of sample on top of solenoid and b) H_z being the external static magnetic field in the z direction. Here x , y and z are the coordinate axes.

The nonmagnetic particles surrounded the paramagnetic particles in a circular way very similar to a flower-shaped colloidal assembly. The red fluorescence polystyrene particles were present at the equator of the paramagnetic particles and paramagnetic particles being at the center in the reflection mode of the microscope. Movies of these colloidal flower assemblies were captured using a Basler camera (Basler A311fc). The dynamics of the colloidal flower formation and its characteristics was then analyzed by using image processing techniques with the help of a commercially available software package (MATLAB) and open source packages such as ImageJ and Virtual Dub.

2.2.2 The transition strength from solid to liquid colloidal dipolar clusters in precessing magnetic fields

Sample Preparation: 1). Colloidal flowers: Two sets of mixtures were prepared with varying particles size. The mixtures are a) paramagnetic particles (diameter $2a = 2.8 \mu\text{m}$) with nonmagnetic fluorescent (red) polystyrene

particles (diameter $2a = 1.0 \mu\text{m}$) and b) paramagnetic particles (diameter $2a = 2.8 \mu\text{m}$) with nonmagnetic fluorescent (yellow-green) polystyrene particles (diameter $2a = 3.1 \mu\text{m}$) immersed in 20 % diluted ferrofluid EMG 707 was prepared in controlled proportions (paramagnetic 1 : nonmagnetic 4 by volume). These mixtures were vigorously shaken to form homogenous mixtures. Using a pipette a small amount ($0.5 \mu\text{l}$) of these mixtures were placed at the center between two sets of pre-cleaned glass cover slips. Extra care was taken while placing the top glass cover slip such that no air bubble exists to reduce drift. 2).

Diamagnetic Clusters: Three sets of mixtures were prepared with nonmagnetic particles varying particle sizes. The mixtures are a) fluorescent (yellow-green) polystyrene particles (diameter $2a = 9.9 \mu\text{m}$) with nonmagnetic fluorescent (yellow-green) polystyrene particles (diameter $2a = 3.1 \mu\text{m}$), b) fluorescent (yellow-green) polystyrene particles (diameter $2a = 3.1 \mu\text{m}$) with nonmagnetic fluorescent (yellow-green) polystyrene particles (diameter $2a = 3.1 \mu\text{m}$) and c) fluorescent (yellow-green) polystyrene particles (diameter $2a = 3.1 \mu\text{m}$) with nonmagnetic fluorescent (pink) polystyrene particles (diameter $2a = 2.0 \mu\text{m}$) immersed in concentrated ferrofluid EMG 707 was prepared in controlled proportions (paramagnetic 1 : nonmagnetic 4 by volume). These mixtures were vigorously shaken to form homogenous mixtures. Using a pipette a small amount $0.5 \mu\text{l}$ of these mixtures was placed at the center between two sets of pre-cleaned glass cover slips.

External Field and Optical Microscopy: The samples were placed on top of a solenoid, shown in Figure (2.2). For the formation of colloidal flowers a static perpendicular field $H_Z 6.5 \text{ mT}$ was applied. Later an external rotating magnetic field $H_{||} 1.62 \text{ mT}$ with angular frequency $\Omega \approx 188 \text{ s}^{-1}$ was applied. For the diamagnetic clusters a rotating magnetic field $H_{||} 1.62 \text{ mT}$ with angular frequency $\Omega \approx 188 \text{ s}^{-1}$ was applied superposed

by a static magnetic field in the z -direction. These samples were observed un-

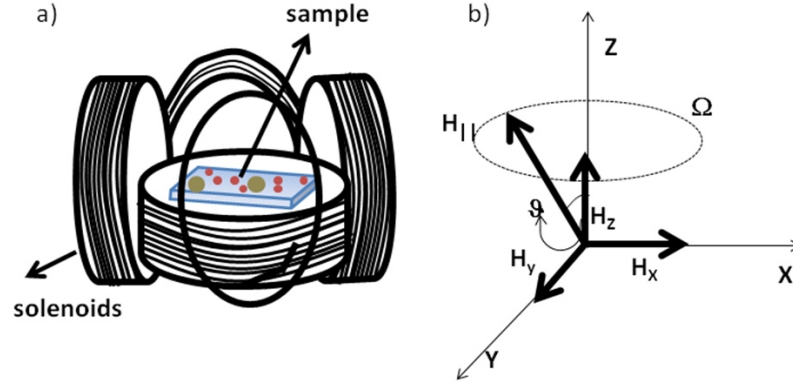


Figure 2.2: a) Schematic representation of arrangements of five sets of solenoid coils and b) the combined rotating magnetic field $H_{||}$ and the perpendicular field H with Ω being the angular frequency and the precession angle θ .

der fluorescence microscope in a reflecting mode. Different colored fluorescence filters were used to observe the fluorescence particles whereas the Polarization filter was used to observe the non-fluorescence paramagnetic particles. Observations and recording: When observed with the different colored fluorescence filters colloidal flowers and clusters were observed. In case of colloidal flowers, the nonmagnetic particles surrounded the paramagnetic particles, which were similar to a flower-shaped colloidal assembly. With the application of the in plane field the diamagnets start to rotate. By varying the perpendicular field the angular frequency of the diamagnets could be altered. At very high static magnetic field 26.0 mT, the flowers have less angular frequency compared to when the static field is low 8.0 mT. In case of diamagnetic clusters, the diamagnets formed isotropic structures similar to the colloidal flowers. In diamagnetic cluster with a high static magnetic field, the angular frequency of the diamagnets around the equator was higher compared to when the field was less. Movies of these colloidal flowers and diamagnetic clusters were cap-

tured using a Leica high-speed camera (Leica DFC 360 FX). The dynamics of the colloidal flowers and clusters formation were analyzed by using image-processing techniques in with the help of a commercially available software package (MATLAB) and open source packages such as ImageJ and Virtual Dub.

2.2.3 Magnetic field controlled composite paramagnetic-diamagnetic colloidal phases

Sample Preparation: A mixture of paramagnetic particles (diameter $2a = 2.8 \mu\text{m}$) with nonmagnetic fluorescent (red) polystyrene particles (diameter $2a = 1.0 \mu\text{m}$) immersed in concentrated ferrofluid EMG 707. was prepared in controlled proportions (paramagnetic 2 : nonmagnetic 4 by volume). This mixture was vigorously shaken to form a homogenous mixture. Using a pipette a small amount $0.5 \mu\text{l}$ of this mixture was placed at the center between two pre-cleaned glass cover slips. External Field and Optical Microscopy: The sample was placed on top of a solenoid, shown in Figure(2.3). A combination of static magnetic field in the z-direction was applied with an in plane time dependent magnetic field . This sample was observed under fluorescence microscope in a reflecting mode. Red fluorescence filter was used to observe the red fluorescence particles whereas the Polarization filter was used to observe the non-fluorescence paramagnetic particles. Observations and recording: Changing the static magnetic field anisotropic structures evolved in 2-dimension and 3-dimension. At high static magnetic field H 26.5 mT colloidal flowers are observed where as decreasing this magnetic field results in forming 3-dimensional anisotropic sandwiched structure. Where the paramagnets are at the middle

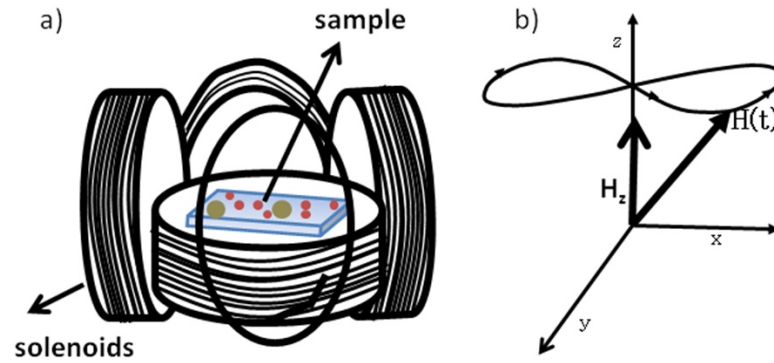


Figure 2.3: a) schematic representation of the arrangement of solenoid coils and b) time dependent magnetic field produced by the five sets of solenoid coils similar to Lissajou curve.

layer and the diamagnets are on the either sides of the paramagnets. Movies of these colloidal flowers, sandwiched structures, decorated strings were captured using a Leica camera (Leica DFC 360 FX).

Chapter 3

Dynamics of self-assembly of flower-shaped magnetic colloidal clusters

**Dynamics of self-assembly of flower-shaped magnetic colloidal
clusters**

A. Ray, S. Aliaskarisohi, and T. M. Fischer,
Phys. Rev. E **82**, 031406 (2010)

Copyright by The American Physical Society 2010

DOI: 10.1140/epje/i2008-10421-5

Dynamics of self-assembly of flower-shaped magnetic colloidal clusters

A. Ray, S. Aliaskarisohi, and T. M. Fischer*

Institute of Physics, Universität Bayreuth, Bayreuth 95440, Germany

(Received 11 May 2010; published 24 September 2010)

In a static magnetic field paramagnetic and nonmagnetic colloids immersed in a ferrofluid self-assemble into fluctuating colloidal flowers. Adsorption and desorption of nonmagnetic petals to larger paramagnetic cores and changes in the petal conformation around the paramagnetic core induce a fluctuating dynamics. We track the motion of colloidal petals on the paramagnetic core. Adsorption and desorption of petals occur on a larger time scale than the rotational diffusion of the petals. Magnetic dipole interactions split the motion of the petals into different modes of rotational diffusion. Modes of rotational diffusion that change the petal conformation are suppressed compared to the conformation invariant rotational diffusion of all petals. The suppression of higher modes of rotational diffusion results in a subdiffusive dynamics of the individual petals.

DOI: [10.1103/PhysRevE.82.031406](https://doi.org/10.1103/PhysRevE.82.031406)

PACS number(s): 82.70.Dd

I. INTRODUCTION

Colloidal assemblies are mesoscopic systems in thermodynamic equilibrium. Understanding the complex structures of these assemblies, the soft interactions between the individual particles, and the resultant dynamics in real space is of current interest; because colloidal assemblies are being used as models for atomic crystals [1] for glasses [2], for van der Waals crystals [3], and as systems for the study of dynamic self-assembly [4,5]. The softness of the interactions gives rise to fluctuations around the equilibrium that allows observing directly the transport processes [6–8] which lead to the dynamic self-assembly of the system. Diffusion is considered as one of these basic passive means for irreversible transport into equilibrium. It arises from fluctuations of the particle velocity due to stochastic forces. These forces act on the diffusing particles due to collisions with other particles from a reservoir at a certain temperature. In the presence of stochastic and deterministic microscopic forces, macroscopic diffusion can be expressed as the zeroth moment of the particle velocity autocorrelation and/or cross-correlation functions [9]. Kubo [9] extended a generalized concept of diffusion that allows defining and measuring the diffusion of interacting particles. It has been shown by Erb *et al.* [5] that paramagnetic and nonmagnetic colloidal particles immersed in a ferrofluid can self-assemble into colloidal flowers in a static magnetic field. The colloidal flowers result from the effective dipolar attraction of the paramagnetic colloids in which nonmagnetic particles behave as magnetic holes in the ferrofluidic background. The dipole interaction is a tensorial traceless interaction that depends on the angle between the magnetic moments and the particle separation. For holes sitting at the pole positions above or below the paramagnetic bead the dipole interaction with the paramagnetic bead is repulsive. In the equatorial plane on the other hand it is attractive. The dipole interaction between two magnetic holes on the other hand is repulsive in the plane normal to the magnetic moments and attractive along the direction of the magnetic moments. The planar structure of the colloidal

flowers is a result of the complex angular dependency of the dipolar interactions.

Here, an attempt has been made to measure the normal modes of diffusion, as well as the adsorption and desorption kinetics of the petals in colloidal flowers using the concept proposed by Kubo [9]. Kubo generalized the concept of diffusions for situations where the particle kinetics is a superposition of random motion and directed interactions that force the particles into deterministic directions. The interactions correlate the motion of the particles that would otherwise show a degenerate individual diffusion. The correlations split the individual diffusion into statistically independent normal modes of diffusion. It is demonstrated that the adsorption and desorption kinetics as well as the mode dependence of the normal modes of petal diffusion can be understood by the competition of dipolar forces with the fluctuating forces from the viscous carrier fluid.

II. EXPERIMENT

We study the superparamagnetic Dynabeads M-270 carboxylic acid, 2.8 μm in diameter (Cat. No. 143.05 D) obtained from Invitrogen Dynal (Oslo, Norway), and Fluro-Max red fluorescent polymer microsphere beads with 1.0 μm diameter (Cat. No. R0100) obtained from Duke Scientific (Palo Alto, CA). The particles from Dynal are supplied in concentrations of approximately 2×10^9 beads ml^{-1} (10–30 mg ml^{-1}) and from Fluro-Max supplied with concentration of approximately 1% volume fraction suspended in water and respective surfactant. Paramagnetic particles are mixed with nonmagnetic particles and diluted ferrofluid EMG 705 FerroTec Ferrosound (FerroTec GmbH, Germany) with controlled proportions depending on the experiment. Electric current of 0.43 A was supplied to the water-cooled coils to produce a magnetic field of 10.0 mT, machined at University of Bayreuth. The mixture of the beads with ferrofluids was taken on a precleaned glass slide with a cover slip to reduce the air drift. Static magnetic field from the z direction was applied to the sample and was observed under the LEICA DM4000B (Leica Microsystems Wetzlar GmbH, Germany) fluorescence microscope through $63\times$ polarization lens in reflecting mode. Videos were cap-

*thomas.fischer@uni-bayreuth.de

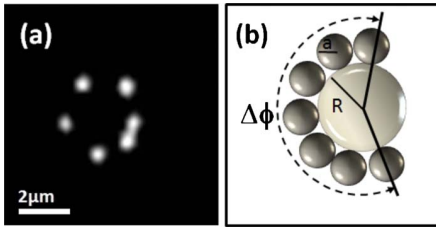


FIG. 1. (Color online) (a) Fluorescence microscope image of a six-petaled colloidal flower and (b) scheme of a colloidal flower. The paramagnetic core particle is nonfluorescent and hence not visible in the fluorescence image. The nonmagnetic fluorescence petal particles are visualized as bright spots in the fluorescence microscope image.

tured using a color charge-coupled device Basler camera (Basler A311fc) high frame rate from Basler AG, Germany.

III. ADSORPTION AND DESORPTION

Nonmagnetic beads of radius $a=0.5 \mu\text{m}$ in a diluted aqueous ferrofluid (EMG 705 Ferrotec Ferrosound/water = 1:4) adsorb at and desorb from the paramagnetic beads of radius $R=1.4 \mu\text{m}$. When they adsorb they form a colloidal flower with one paramagnetic bead at the core of the flower surrounded by several nonmagnetic beads forming the petals. A typical colloidal flower is depicted in Fig. 1. The assembly is a dynamic structure and the number of petals $N(t)$ fluctuates as a function of time because nonmagnetic beads adsorb at and desorb from the paramagnetic core. If we assume a Boltzmann distribution for the number of petals we may extract the potential energy of adsorption of N beads $U(N)$ as

$$U(N) - U(N_{\text{ref}}) = -k_B T \ln \left(\frac{t(N)}{t(N_{\text{ref}})} \right), \quad (1)$$

where $t(N)$ denotes the total time when one finds the colloidal flower with N petals, N_{ref} denotes a reference number of petals, and T is the temperature. In Fig. 2 we plot the adsorp-

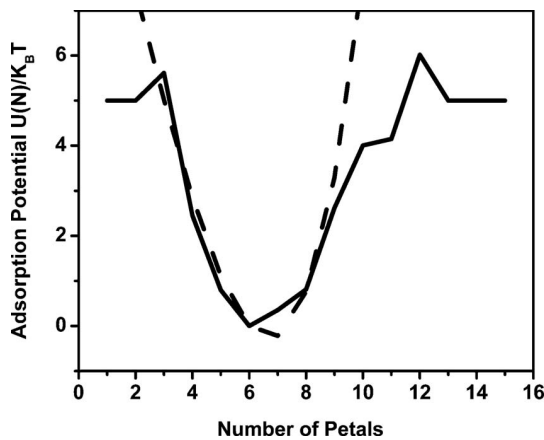


FIG. 2. Adsorption potential of the colloidal petals. The solid line is obtained from the experimental data by using Eq. (1). This potential levels off near $5k_B T$ due to lack of events. The dashed line is a fit according to Eq. (2).

tion potential as a function of the number of petals obtained via Eq. (1) by measuring $N(t)$ over a time duration of 4000 video frames. The adsorption potential shows a pronounced minimum near six petals. Assuming the potential to arise via dipolar attraction of the nonmagnetic beads to the paramagnetic core and due to dipolar repulsion between the equally spaced nonmagnetic petals, we predict a potential of

$$U(N) = \frac{4\pi\mu_0\chi_F^2 H^2 a^3}{9(R/a+1)^3} N \left[-\left(\frac{\chi_p}{\chi_F} - 1\right) \frac{R^3}{a^3} + \frac{1}{2} \sum_{j=1}^{N-1} \frac{1}{8 \sin^3(j\pi/N)} \right]. \quad (2)$$

In Eq. (2) μ_0 denotes the vacuum permeability, χ_F and χ_p are the effective susceptibilities of the ferrofluid and of the paramagnetic particle, and H is the external magnetic field. The potential has a minimum for an equilibrium number of particles given approximately by

$$N_{eq} = \frac{2\pi}{\sqrt{3}} \sqrt{\frac{\chi_p}{\chi_F} - 1} \frac{R^{3/2}}{a^{3/2}}. \quad (3)$$

The dashed line in Fig. 2 shows a fit of the experimental data (solid line) obtained from Eq. (1) to the theoretical prediction in Eq. (2) using $\chi_p=0.082$ and $\chi_F=0.063$. Note that the theoretical fit exhibits a minimum around $N=7$ instead of the value $N=6$ in the experiment.

The $2N$ -dimensional conformational space of the petals is spanned by the positions $(r_j, \varphi_j, j=1, \dots, N)$ of the petals. In an N -fold colloidal flower the equilibrium configuration is determined by the conformation $r_j=R+a$ and $\varphi_j=2\pi j/N$ ($j=1, \dots, N$). A transition to a $(N-1)$ -fold flower happens when, for example, the N th petal separates from the flower ($r_N \rightarrow \infty$) and the remaining $N-1$ petals rearrange their angular positions φ_j ($j=1, \dots, N-1$). We describe the reaction pathway of such a conformational change by the reaction coordinate Δr . The position of the N th petal is $r_N=R+a+\Delta r_N$, $\varphi_N=0$ and the other beads adapt the positions $r_j=R+a$, $\varphi_j=\alpha(\Delta r_N)+2[\pi-\alpha(\Delta r_N)](j-1)/(N-2)$. The angle $2\alpha(\Delta r_N)$ describes the angle between the first and the $(N-1)$ th petals that readjust [from $\alpha=2\pi/N$ to $\alpha=\pi/(N-1)$], while the N th petal leaves the flower (see top in Fig. 3). We compute the reaction pathway such that the remaining petals $j=1, \dots, N-1$ adjust their positions to the energy minimum of the dipolar energy of the N petal system while the N th petal is fixed at the position $r_N=R+a+\Delta r_N$. Usually no significant changes in energy are computed when the separation Δr_N of the leaving petal has exceeded $\Delta r_N > 4 \mu\text{m}$. Hence, separations larger than $4 \mu\text{m}$ can be considered as quasi-infinite separations. In Fig. 3 we plot the dipolar energy versus the reaction coordinates Δr_N ($N=3, \dots, 11$) for a cascade of transitions from an 11-fold colloidal flower toward a flower with two petals. The cascade from the 11-folded flower to the theoretical minimum flower with seven petals is plotted on the left side. The remaining cascade from the minimum sevenfold flower toward a two-petal flower is plotted at the right. The reaction coordinates alternate between the lower (even N) and upper

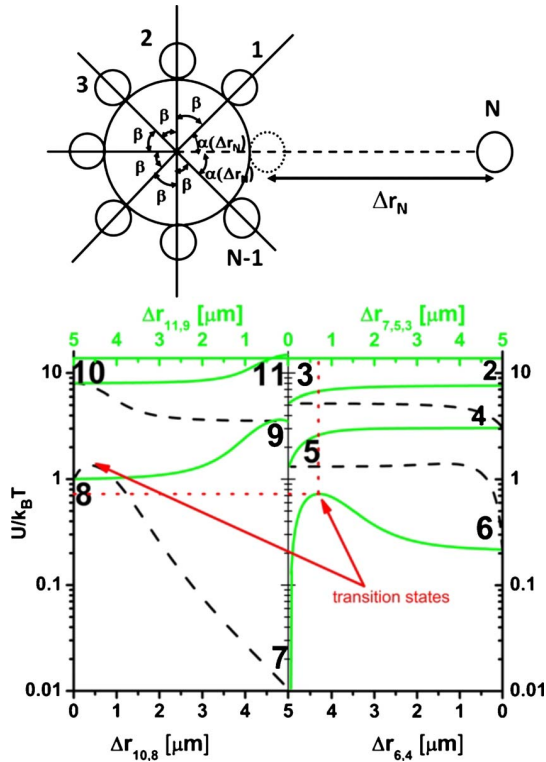


FIG. 3. (Color online) (Top) Scheme of a N -petaled flower losing the N th petal along the reaction coordinate Δr_N , while the angular positions of the remaining petals adjust. (Bottom) The potential-energy cascade from a 11-petaled flower via the stable VII petal flower (left) toward a two-level flower (right). The flower loses the N th petal along the reaction coordinate Δr_N ; black curves correspond to the desorption of a N -even petal (lower abscissa), and green (gray) curves correspond to the desorption of a N -odd petal (upper abscissa). The energy of a petal separated by $\Delta r_N = 5 \mu\text{m}$ is indistinguishable from an infinitely separated petal and hence equals to the energy of a $(N-1)$ -petaled flower. The numbers labeling the ends of the curves correspond to the number of the petals in the flower. The transition state between sixfold and sevenfold petal flowers [red (black) arrow] is at a distance of $\Delta r = 0.7 \mu\text{m}$ from the equilibrium position of the seventh petal and has an activation energy of $E_A = 0.7k_B T$.

(odd N) axes. Numbers indicate equilibrium flowers of the corresponding number of petals. The potential thus changes from the N petal flower energy E_N to the $(N-1)$ petal flower energy E_{N-1} . The potential of a N petal flower with the N th petal at a distance $\Delta r = 5 \mu\text{m}$ is indistinguishable from the potential energy of a $(N-1)$ -petaled flower. This confirms that a petal at a distance $\Delta r > 5 \mu\text{m}$ can be considered as fully separated from the flower. For the desorption of the seventh petal the energy exhibits a maximum E_A along the reaction pathway. This maximum corresponds to a transition state, i.e., a saddle point in conformational space located at a distance $\Delta r_{7,max} \approx 0.7 \mu\text{m}$ from the minimum position of the seventh petal with an activation barrier of the desorption of $(E_A - E_7) \approx 0.7k_B T$. The activation energy for the adsorption is $(E_A - E_6) \approx 0.5k_B T$. A qualitatively similar transition state is computed between the seven- and eight-petaled flowers. All other transitions in the number of petals show no transi-

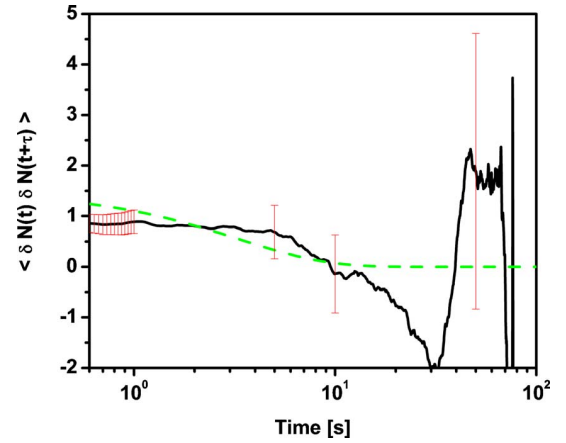


FIG. 4. (Color online) The autocorrelation function $\langle \delta N(t) \delta N(t+\tau) \rangle$ versus time as obtained from the experimental data (solid line). The number of petals changes on a time scale of 3 s. The dashed line corresponds to an exponential decay with rate constant 0.3 s^{-1} . The statistical error (error bars) of the correlation function increases when the time lag τ approaches the time of measurement $\tau_{meas} = 70 \text{ s}$.

tion state. Hence, all flowers with $N < 6$ and $N > 8$ are unstable. The six- and eight-petaled flowers are metastable $E_6, E_8 > 0$, and the sevenfold flower is the stable conformation $E_7 = 0$ for the given parameter set. Assuming an Arrhenius behavior for the rate constant $k_{6 \rightarrow 7}$ of the adsorption process of the seventh petal one would expect a rate constant of the order

$$k_{6 \rightarrow 7} = \frac{k_B T}{6 \pi \eta a} (\Delta r_{max})^{-2} \exp[-(E_A - E_6)/k_B T], \quad (4)$$

where $\eta = 10^{-3} \text{ N s m}^{-2}$ is the ferrofluid viscosity. Inserting the values $\Delta r_{max} \approx 0.7 \mu\text{m}$ and $(E_A - E_6) \approx 0.5k_B T$ from Fig. 3 into Eq. (4) we obtain $k_{6 \rightarrow 7} \approx 0.3 \text{ s}^{-1}$. In Fig. 4 we plot the autocorrelation function of the petal number,

$$\langle \delta N(t) \delta N(t+\tau) \rangle, \quad (5)$$

where $\delta N(t) = N(t) - N_{eq}$ denotes the petal number fluctuation. The autocorrelation function decays with a typical rate of $k_{ex} \approx 0.3 \text{ s}^{-1}$ in good agreement with the estimate given by Eq. (4). For larger times $\tau > 10 \text{ s}$ the experimental autocorrelation function becomes statistically unreliable since the number of events ($\propto \tau_{meas} - \tau$) drops to 1 as the time separation τ approaches the time τ_{meas} of the measurement.

IV. PETAL CONFORMATION AND DYNAMICS

Once the petals adsorb to the paramagnetic core there is some freedom of conformation, and one observes flowers with petals equally spaced around the core as well as conformations where the petals are crowded at one side of the core. We define the one-dimensional density of particles as

$$\rho = N/\Delta\phi, \quad (6)$$

where $\Delta\phi$ denotes the minimum angular range over which the N petals are distributed and $2\pi - \Delta\phi$ is the largest gap

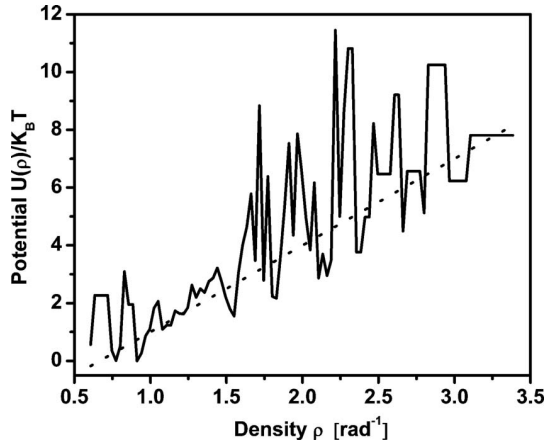


FIG. 5. Effective petal potential as a function of the petal density ρ as obtained from the experimental data via Eq. (7). The dashed line is a linear fit.

between the petals. We compute the potential energy of a conformation $U(\rho)$ as

$$U(\rho) - U(\rho_{ref}) = -k_B T \ln \left(\frac{g(\rho_{ref}) \Delta \rho_{ref} t(\rho, \Delta \rho)}{g(\rho) \Delta \rho t(\rho_{ref}, \Delta \rho_{ref})} \right), \quad (7)$$

where $t(\rho, \Delta \rho)$ is the total time when the petals in the flower show a density in the interval $[\rho, \rho + \Delta \rho]$ and where

$$g(\rho) \propto \left(\frac{N}{\rho} - \frac{N}{\rho_{hc}} \right)^{N-2} \quad (8)$$

is the leading-order approximation for the configurational space density [10] available for conformations of density ρ , whereas $\rho_{hc} = (R/a+1)/2$ is the maximum (hard-core) packing density of the petals around the core. Figure 5 shows the potential $U(\rho)$ computed via Eq. (7) for flowers consisting of an arbitrary number of petals. The resolution $\Delta \rho$ varies with ρ and is chosen in a way so as to ensure that $t(\rho, \Delta \rho) > 0$ for all ρ . Since the data at higher potential are sparse the resolution $1/\Delta \rho$ is best at the minimum and decreases when moving toward higher potential. We find the lowest potential for densities $\rho \approx 1$ corresponding to a hexagonal arrangement of the petals with equal spacing of $\pi/3$ between the petals. The petal conformation results from the simultaneous minimization of the petal number and the minimization of the dipolar repulsion between the petals. The dipolar repulsion between the petals, however, is weak and allows for significant fluctuations around a conformation. We therefore tracked the angular position $\phi_j(t)$ [$j=1, 2, 3, \dots, N(t)$] of the adsorbed petals as a function of time. The accuracy of the tracking of $\phi_j(t)$ was better than 2° . The angular frequency $\omega_j(t) = \dot{\phi}_j(t)$ of each individual petal is a fluctuating function of time. We measure the angular frequency using finite differences of the angular positions of consecutive frames. The frame rate of the camera was 30 frames per second. We define the autocorrelation function of the angular frequency of two petals of a colloidal flower with N petals as

$$C_N(\sigma, \tau) = \langle \omega_j(t) \omega_{j \pm \sigma}(t + \tau) \delta(N(t) - N) \delta(N(t + \tau) - N) \rangle. \quad (9)$$

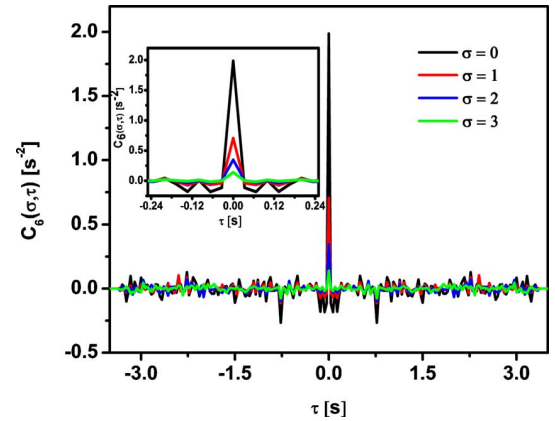
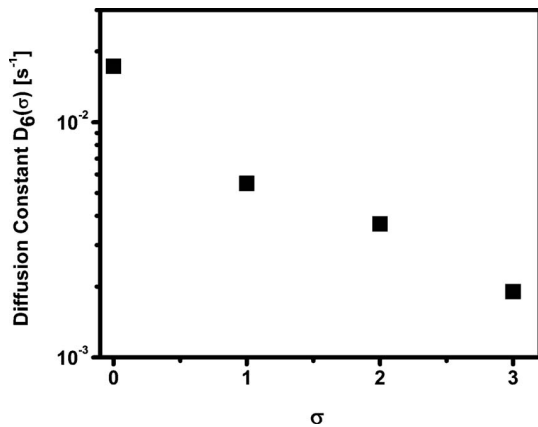


FIG. 6. (Color online) Angular frequency autocorrelation and cross-correlation functions for a colloidal flower with six petals. The black line corresponds to the autocorrelation, while the red, blue, and green lines correspond to cross correlations between nearest ($\sigma=1$), second-nearest ($\sigma=2$), and third-nearest ($\sigma=3$) neighbors, respectively.

Here, σ denotes the neighbor number ($\sigma=0$ is the same particle, $\sigma=1$ is the nearest neighbor, etc.). Both delta functions $\delta(N(t)-N)$ and $\delta(N(t+\tau)-N)$ discard all times where the petal number deviates from the fixed petal number N from the correlation.

In Fig. 6 we plot $C_6(\sigma, \tau)$ versus τ for $\sigma=0, 1, 2, 3$. The angular frequencies are correlated for zero time delay (i.e., $\tau=0$), showing that part of the petal diffusion can be considered as a Markovian process on the time scale $\tau > 0.03$ s of the measurement. The most prominent observation is that neighboring petals are not statistically independent. As does the petal autocorrelation function $C_6(0, \tau)$, the petal cross-correlation functions $C_6(\sigma \neq 0, \tau)$ also show the same albeit weaker instantaneous positive correlation. This is a dynamic proof of the deterministic interaction of the petals. Apart from this positive correlation a weak anticorrelated decay is observed for the autocorrelation $C_6(0, \tau)$ and the cross correlation $C_6(\sigma \neq 0, \tau)$ for $\tau > 0.05$ s (see the inset in Fig. 6). It is a measure for the retardation of the interaction. In single file diffusion [11–13], where particles interact only via hard-core repulsion, a strong algebraic anticorrelation significantly alters the diffusion of the particles. Neighboring particles in single file diffusion remain uncorrelated at short times and become anticorrelated only at times typical for the individual diffusion time needed to encounter each other. The retardation of such a hard-core interaction is significant. Single file diffusion becomes most prominent in the thermodynamic limit $N \rightarrow \infty$, where the time scale of the simultaneous correlated diffusion of the rigid flower separates from the individual diffusion of the petals.

Our system differs from a system exhibiting single file diffusion. It has a small number of petals, and the petals interact instantaneously via the soft dipolar interactions; retardation effects are weak. In no time are the petals allowed to diffuse individually. Hence, the relatively weak delayed anticorrelation follows the instantaneous delta correlation with a relative short delay. The diffusion constant of the petals is given by half the area under the autocorrelation func-

FIG. 7. Diffusion constant $D_G(\sigma)$ versus σ .

tion. While the finite frame rate of the camera broadens the experimental correlation function, the area under the correlation function is not affected by the convolution of the data with the time resolution function of the camera. Hence, the diffusion constants have no significant dependence on the frame rate of recording,

$$D_N(\sigma) = \int_0^\infty d\tau C_N(\sigma, \tau). \quad (10)$$

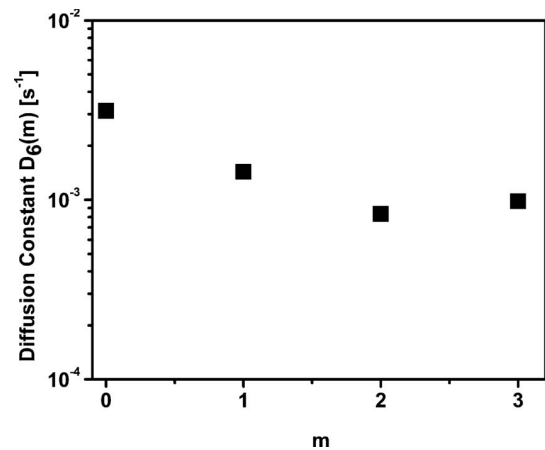
Equation (10) is Kubo's [9] generalization of the concept of diffusion to particles that interact. The interaction of the particles causes the motion of one particle to statistically depend on the motion of another. The statistically dependent motion of the particles can be decomposed into statistically independent normal modes of motion. In Fig. 7 we plot the diffusion constant $D_G(\sigma)$ versus σ . The petals behave like being coupled by soft springs, with petals not diffusing independently, but with neighbors performing a correlated diffusion. The correlation decreases when moving away toward further distant neighbors. We may decompose the correlated motion of the petals into uncorrelated normal modes of diffusion via

$$\phi(m, t) = \frac{1}{\sqrt{N}} \sum_{j=1}^N e^{2\pi i m j / N} \phi_j(t). \quad (11)$$

The corresponding statistically independent diffusion constants of the normal modes,

$$D_N(m) = \frac{1}{N} \sum_{\sigma=1}^N e^{2\pi i m \sigma / N} D_N(\sigma), \quad (12)$$

are plotted in Fig. 8. The mode $m=0$ has the highest diffusion constant, and the diffusion constant decreases with the mode number m . The mode $m=0$ corresponds to a rigid ro-

FIG. 8. Normal-mode diffusion constants $D_G(m)$ versus the mode number m .

tation of all petals by the same amount. It therefore corresponds to the rotational diffusion of the entire flower that leaves the conformation of the flower unchanged. The higher modes $m > 0$ involve relative motion of petals that change the conformation. Such modes are suppressed to diffuse by the dipolar repulsion between the petals. The higher is m , the shorter is the distance $2\pi/m$ between petals that are moving in opposite directions. The most likely conformation is an equilibrium conformation such that an $m \neq 0$ mode usually raises the dipolar energy of the system. This explains why the diffusion of higher modes $|m| > 0$ is suppressed by the dipole-dipole interaction.

Contrary to single file diffusion the diffusion mode of the petals arises from mostly instantaneous response of the flower to conformational changes. In single file diffusion the suppression of higher modes arises from a retarded response to conformational changes that only sets in when one petal diffuses to its neighbor and encounters its hard-core repulsion.

In conclusion we have characterized the dynamic fluctuations of magnetic colloidal flowers. These fluctuations can be understood as a result of deterministic forces arising due to dipolar interactions and statistical forces arising from the collisions of the embedding fluid. The soft character of the dipolar interactions places this system between that of a free system and a system interacting via hard-core interactions. The soft confinement of the particles leads to a mode-dependent diffusion that differs from single file diffusion. The desorption and adsorption of the petals can be understood as activated processes. The colloidal flowers are thus a two-dimensional model system for the dynamics of more complex three-dimensional colloidal assemblies such as Pickering emulsions [14] and colloidosomes [15].

- [1] A. van Blaaderen, R. Ruel, and P. Wiltzius, *Nature (London)* **385**, 321 (1997).
- [2] E. R. Weeks, J. C. Crocker, A. C. Levitt, A. Schofield, and D. A. Weitz, *Science* **287**, 627 (2000).
- [3] N. Osterman, I. Poberaj, J. Dobnikar, D. Frenkel, P. Ziherl, and D. Babić, *Phys. Rev. Lett.* **103**, 228301 (2009).
- [4] P. Tierno, R. Muruganathan, and Th. M. Fischer, *Phys. Rev. Lett.* **98**, 028301 (2007).
- [5] R. M. Erb, H. S. Son, B. Samanta, V. M. Rotello, and B. B. Yellen, *Nature (London)* **457**, 999 (2009).
- [6] K. Schätzel and B. J. Ackerson, *Phys. Rev. E* **48**, 3766 (1993).
- [7] E. Vignati, R. Piazza, and T. P. Lockhart, *Langmuir* **19**, 6650 (2003).
- [8] Y. Terada and M. Tokuyama, *J. Phys. Soc. Jpn.* **79**, 034802 (2010).
- [9] R. Kubo, *J. Phys. Soc. Jpn.* **12**, 570 (1957).
- [10] The assumption that $2\pi - \Delta\phi$ is the largest gap forbids conformations with density ρ that have a larger gap between the first and N th petals. Three particle correlations of this kind have been neglected when approximating the conformational space density $g(\rho)$. The systematic error introduced in this way cancels near the potential minimum due to the normalization with $g(\rho_{ref})$.
- [11] Q. H. Wei, C. Bechinger, and P. Leiderer, *Science* **287**, 625 (2000).
- [12] J. Kärger, *Phys. Rev. A* **45**, 4173 (1992).
- [13] V. Kukla, J. Kornatowski, D. Demuth, I. Gimus, H. Pfeifer, L. V. C. Rees, S. Schunk, K. K. Unger, and J. Kärger, *Science* **272**, 702 (1996).
- [14] R. Aveyard, B. P. Binks, and J. H. Clint, *Adv. Colloid Interface Sci.* **100-102**, 503 (2003).
- [15] A. D. Dinsmore, M. F. Hsu, M. G. Nikolaides, M. Marquez, A. R. Bausch, and D. A. Weitz, *Science* **298**, 1006 (2002).

Chapter 4

Core size effects on the rotation
and stability of dipolar clusters in
precessing magnetic fields

**Core size effects on the rotation and stability of dipolar clusters in
precessing magnetic fields**

A. Ray and T. M. Fischer,
Eur. Phys. J. E (2012) **35**: 17

Copyright by The European Physical Journal E 2012

DOI: [10.1140/epje/i2012-12017-x](https://doi.org/10.1140/epje/i2012-12017-x)

EPJ E

Soft Matter and
Biological Physics

EPJ.org
your physics journal

Eur. Phys. J. E (2012) **35**: 17

DOI 10.1140/epje/i2012-12017-x

Core size effects on the rotation and stability of dipolar clusters in precessing magnetic fields

A. Ray and T.M. Fischer



Società
Italiana
di Fisica



Springer

The transition strength from solid to liquid colloidal dipolar clusters in precessing magnetic fields*

A. Ray and Th.M. Fischer^a

Institut für Experimentalphysik, Universität Bayreuth, 95440 Bayreuth, Germany

Received 6 October 2011 and Received in final form 31 January 2012

Published online: 9 March 2012

© The Author(s) 2012. This article is published with open access at Springerlink.com

Abstract. We report on the rotation of colloidal clusters of diamagnetic beads and of mixtures of paramagnetic and diamagnetic beads in a ferrofluid in a precessing external magnetic field. The precession angle of the external field is a control parameter determining the stability of the cluster. Clusters become locally unstable when the local precession angle reaches the magic angle. Cluster shape dependent depolarization fields lead to a deviation of the local from the external precession angle such that close to the external magic angle different cluster shapes might coexist. For this reason cluster transitions are weakly or strongly first-order transitions. If the transition is weakly first order a critical speeding up of the cluster rotation is observed. No speeding up occurs for strongly first-order cluster transitions with hysteresis. The strength of the first-order transition is controlled by the size of the core of the cluster.

1 Introduction

The formation of a solid from an assembly of particles is a result of the strength, range and form of attractive particle interactions. In this respect colloidal particles have evolved into a rich model system. The interactions between two pairs of colloids are often known quantitatively and the resulting structure [1,2] can be viewed with microscopic techniques. Amongst the variety of different colloids paramagnetic colloids are one special class of colloids that interact via long-range dipole interactions. The orientation-dependent tensor form of the dipole interactions results in complex static [3] and dynamic [4] structures that can be formed from paramagnetic colloids. Dipole interactions switch from attractive to repulsive depending on whether

the magnetic dipole moments are oriented longitudinal or transversal with respect to the particle separation. This orientation dependence of the dipolar interactions can be further exploited by using time-dependent magnetic fields with large Mason number [5] that vary on a time scale too fast for the colloids to relax to their instantaneous equilibrium position [3,6,7]. The colloids therefore experience the time-averaged dipolar interactions. These are attractive in those directions where the frequency of longitudinal orientations of the induced magnetic moment is larger than half the frequency of the two transversal orientations. For an isotropic fluctuation with equal probabilities of longitudinal and the two transversal orientations the average dipole interaction vanishes. One of the simplest time-dependent magnetic fields is a precession of the magnetic field around an axis with precession angle ϑ . For such precession, the frequencies of longitudinal and transversal orientations become similar at the magic angle [8] $\vartheta_{\text{magic}} = 54.7^\circ$ and dipole interactions switch sign. For precession angles below the magic angle the dipole interactions are attractive along the precession axis [9] and repulsive in the plane perpendicular to it. For larger angles we have the opposite behaviour. Dipole interactions are similar for the interaction of diamagnetic particles the magnetic moment of which point in the opposite direction than for paramagnets. Dipole interactions, however, switch sign when one looks at the interaction of paramagnetic and diamagnetic particles. A paramagnet in a precessing field will attract other paramagnets along the precession axis and diamagnets in the plane perpendicular to the precession axis if the precession angle is below magic.

* Supplementary material in the form of an avi file available from the Journal web page at

<http://dx.doi.org/10.1140/epje/i2012-12017-x>

Supplementary.avi is a movie showing the rotation of the colloidal flowers and diamagnets of figure 1 at precession angles close and far from the magic angle. Top two rows of movies are colloidal flowers. The first row is close to the magic angle. The second row of movies shows the same flowers at a lower angle. Bottom two rows of movies are colloidal diamagnetic clusters. The third row shows the colloidal clusters close to the magic angle, the fourth row shows the same colloidal clusters at a higher precession angle. The core size ratio increases for both the colloidal flowers and for the colloidal clusters from the left toward the right. The ratio of the rotation speed of similar flowers and clusters decreases at the same time.

^a e-mail: thomas.fischer@uni-bayreuth.de

One can prepare effective diamagnetic colloids by immersing non-magnetic colloids, so-called magnetic holes, into a ferrofluid. The interaction of effective diamagnets with paramagnets leads to the formation of flower shaped clusters [10] with a paramagnetic core surrounded by diamagnetic petals. In our present experiments magnetic colloidal holes and paramagnetic colloids are placed in a thin film of ferrofluid between to glass plates. The magnetic ferrofluid glass boundaries give rise to virtual image dipoles suppressing any further attraction of beads of any kind along the film normal and assembly mainly happens in the plane. We assembled different planar clusters of effective diamagnets and of a mixture of effective diamagnets and paramagnetic beads in a ferrofluid film subject to a precessing field. Amongst the clusters formed here we focus on clusters that are isotropic in the film plane. Isotropic clusters of diamagnetic beads form above the magic angle while colloidal flowers with a paramagnetic core surrounded by diamagnets form below the magic angle. Both clusters fall apart when approaching the magic angle from different sides (from above and below, respectively), and the precession angle serves as a control parameter for the stability of the clusters. If the orientation of the magnetic dipoles of each particle were oriented along the direction of the external magnetic field then dipolar interactions would be proportional to the second Legendre polynomial of the precession angle of the external field and therefore continuously decrease to zero when approaching the magic angle. From such a picture one would assume the transition from a cluster toward a colloidal liquid to be of second order. However, the local field at the position of one colloidal particle is a superposition of the external field with the depolarization field resulting from the magnetic moments of the other particles and therefore the local field is generically oriented into a direction different from the external field. An individual particle will hence precess with an angle, different then the precession angle of the external field. The deviation of the local from the external precession angle can self-consistently stabilize or destabilize a certain cluster shape. It is for this reason possible that different structures can be locally stable at the same time. One then observes a coexistence of clusters with a liquid. Depolarization from third particles will therefore in general render the cluster stability/instability transition into a first order transition. The current work focuses on the question of the strength of order of the cluster stability transition. We will show that for clusters consisting of one central core particle and a one-particle thick ring of particles surrounding the core particle, the ratio of the core particle radius to the ring particle radius determines how strongly or weakly the transition is of first order.

A second order transition is a transition where the order parameter changes continuously at the transition. A first order transition exhibits a discontinuous change of the order parameter. The change of one phase to the other occurs via a coexistence of the two phases. The area of the hysteresis measures the dissipated energy when traversing the coexistence region back and forth. Second order transitions are associated with a critical behaviour of response

functions as a function of the control parameter, while first order transitions exhibit no critical behaviour.

Here we measure the angular velocity of isotropic colloidal clusters in a ferrofluid that occurs as a response to an external precessing field. As a function of the external precession angle this angular velocity shows a critical speeding up for clusters undergoing a weakly first-order transition to a colloidal liquid with a small hysteresis, while clusters undergoing a strong first-order transition with a large hysteresis show no critical speeding up.

The anisotropic part of the susceptibility tensor of isotropic cluster vanishes such that there is no magnetic torque on the cluster arising due to a preferential orientation of the cluster. The only magnetic torque acting on isotropic clusters is exerted via a memory effect in the contrast of the cluster to surrounding susceptibility. The magnetization in the sample lags behind the magnetic field in both the ferrofluid and in the cluster such that the non-vanishing angle between magnetization and magnetic field results in a magnetic torque in both the ferrofluid and in the cluster. The background torque in the ferrofluid is balanced by the sample wall and the positive or negative excess torque on the cluster results in a steady asynchronous co- or counter rotation of the cluster. The cluster susceptibility of isotropic clusters is a shape-independent isotropic tensor that reflects the interactions that keep the cluster intact. The angular frequency of rotation of the clusters is therefore an ideal measure for the self-consistent interactions that keep the integrity of the cluster.

2 Experimental

For the study of the dynamical behavior of the colloidal flowers and colloidal clusters we used superparamagnetic Dynabeads M-270 functionalized with carboxylic acid (Invitrogen Dynal Oslo, Norway) of diameter $a = 2.8 \mu\text{m}$ and effective susceptibility $\chi = 0.8$, non-magnetic carboxylate-coated yellow-green fluorescence polystyrene particles of diameter $2.0 \mu\text{m}$ from FluroMax, red fluorescent polystyrene microspheres of diameter $2a = 1.0 \mu\text{m}$ from Duke Scientific (Palo Alto, CA) and green fluorescence polystyrene particles with diameters $2a = 3.1 \mu\text{m}$ and $2a = 9.9 \mu\text{m}$ were obtained from ThermoScientific.

For colloidal flowers the paramagnetic and non-magnetic particles were immersed in diluted ferrofluid EMG 707 FerroTec Ferrosound (FerroTec GmbH, Germany) with controlled proportions (EMG 707 : H₂O = 20 : 80) depending on the experiment and sandwiched between two cover slips of a separation of roughly $100 \mu\text{m}$. The susceptibility of EMG 707 is $\chi_F = \phi_F \phi_P \chi_{\text{magnetite}}$, with $\chi_{\text{magnetite}} = 21$ the susceptibility of bulk magnetite, $\phi_P = 2\%$ the volume fraction of magnetite nanoparticles in the undiluted ferrofluid and $\phi_F = 1$ ($\phi_F = 0.2$) the volume fraction of ferrofluid in the ferrofluid water mixture. The cover slip was then subjected to static magnetic field, produced by a coil mounted under the sample. Colloidal flowers are formed and these flowers are then placed in a rotating field produced by pairs of Helmholtz coils and was observed with

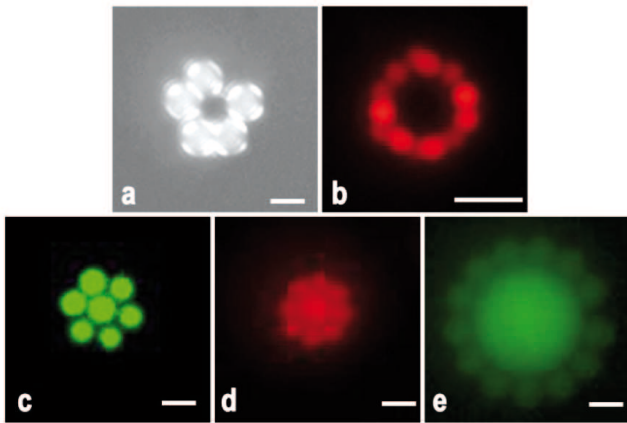


Fig. 1. a)-b) Reflection polarization—respectively, fluorescence—microscope image of a colloidal flower consisting of a paramagnetic (non-fluorescent) core of diameter $2a_1 = 2.8 \mu\text{m}$ in an aqueous diluted ferrofluid (EMG707 : $\text{H}_2\text{O} = 20 : 80$) surrounded by an isotropic ring of diamagnets of diameter a) $2a_2 = 3.1 \mu\text{m}$ and b) $2a_2 = 1.0 \mu\text{m}$. The images were obtained in a normal field of $\hat{H}_\perp = 7 \text{ mT}$. c)-e) Fluorescence microscope images of isotropic clusters of diamagnets of diameter c) $2a_1 = 3.1 \mu\text{m}$ and $2a_2 = 3.1 \mu\text{m}$, d) $2a_1 = 3.1 \mu\text{m}$ and $2a_2 = 2.0 \mu\text{m}$ and e) $2a_1 = 9.9 \mu\text{m}$ and $2a_2 = 3.1 \mu\text{m}$, immersed into an undiluted ferrofluid (EMG 707). The clusters were assembled in an in-plane rotating field of $\hat{H}_\parallel = 1.62 \text{ mT}$ at a precession angular frequency of $\Omega = 188 \text{ s}^{-1}$. The scale bar in all images corresponds to $3 \mu\text{m}$. The movie in the supporting information shows the rotating clusters under the in-plane field of $\hat{H}_\parallel = 1.62 \text{ mT}$ and two different normal fields with a precession angle close and far from the magic angle.

fluorescence or reflection microscopy, LEICA DM5000 (Leica Microsystems Wetzlar GmbH, Germany).

For colloidal clusters non-magnetic particles with different size diameters were immersed in undiluted ferrofluid EMG 707 sandwiched between two cover slips. The cover was then subjected to a rotating magnetic field where isotropic colloidal clusters are formed. Then a static magnetic field normal to the film was superposed to the rotating in-plane field and the dynamics of the clusters were observed under the fluorescence microscope.

The field direction of the magnetic field changes from the air into the ferrofluid film according to $\hat{H}_\perp^{\text{ferrofluid}} = \hat{H}_\perp^{\text{air}} / (1 + \chi_F)$ and $\hat{H}_\parallel^{\text{ferrofluid}} = \hat{H}_\parallel^{\text{air}}$, and the precession angle in the ferrofluid and in the air are related via $\tan \vartheta^{\text{ferrofluid}} = (1 + \chi_F) \tan \vartheta^{\text{air}}$. χ_F denotes the magnetic susceptibility of the ferrofluid. All external fields and external precession angles are given in terms of their values inside the ferrofluid.

3 Results

Isotropic colloidal flowers were assembled in a static magnetic field normal to the sample consisting of a mixture of paramagnetic and non-magnetic particles dispersed in a

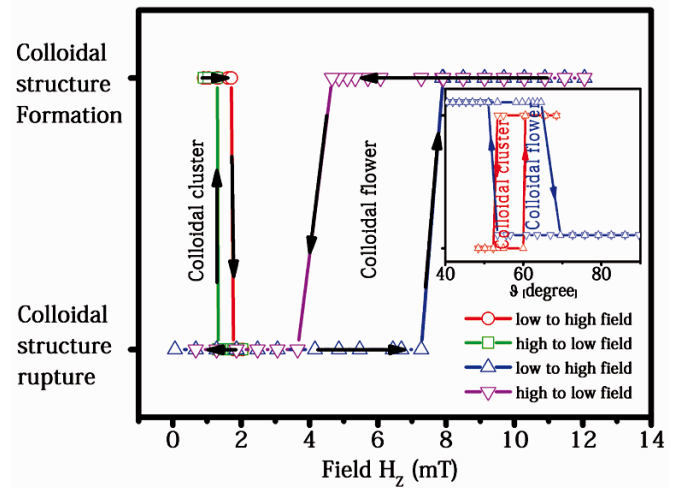


Fig. 2. (Colour on-line) Hysteresis loops of the formation and rupture of colloidal flowers and of diamagnetic clusters as a function of the static normal field \hat{H}_\perp . The colloidal flowers consisted of a paramagnetic (non-fluorescent) core of diameter $2a_1 = 2.8 \mu\text{m}$ in an aqueous diluted ferrofluid (EMG 707 : $\text{H}_2\text{O} = 20 : 80$) surrounded by an isotropic ring of diamagnets of diameter $2a_2 = 1 \mu\text{m}$ in a rotating field of $\hat{H}_\parallel = 1.62 \text{ mT}$ at a precession angular frequency of $\Omega = 188 \text{ s}^{-1}$. Blue upward triangles correspond to increasing the normal field and pink downward triangles to decreasing normal field. The diamagnetic clusters consisted of core particles of diameter $2a_1 = 3.1 \mu\text{m}$ and petals of diameter $2a_2 = 3.1 \mu\text{m}$ immersed in an aqueous undiluted ferrofluid (EMG 707). The rotating in-plane field strength and frequency were the same as for the colloidal flowers. Red circles are measured upon increasing and the green squares upon decreasing the normal field. The inset shows the same hysteresis loops in terms of the precession angle.

diluted ferrofluid. It has been shown [11,12] that with the proper dilution the magnetic susceptibility can be tuned to prefer a number of diamagnetic petals absorbing at the magnetic core corresponding to a full monolayer of petals around the core. Such kinds of isotropic colloidal flowers are displayed in fig. 1a)-b). Clusters of a bidisperse (radii a_1 and a_2) mixture of effective diamagnets in a ferrofluid were formed in an in-plane rotating magnetic field. The diamagnetic clusters formed are planar clusters lying in the mid plane of the ferrofluid sample having a rich variety of conformations with different numbers of diamagnets forming one clusters. Amongst this variety we picked out clusters having a core formed by a bead of radius a_1 surrounded by a complete monolayer of beads with radius a_2 . Examples of such isotropic diamagnetic clusters are shown in fig. 1c)-e).

Both types of clusters were exposed to a precessing magnetic field being a superposition of a rotating magnetic field $\mathbf{H}_\parallel(t) = \hat{H}_\parallel [\mathbf{e}_x \cos \Omega t + \mathbf{e}_y \sin \Omega t]$ in the plane of the ferrofluid film and a static field $\mathbf{H}_\perp(t) = \hat{H}_\perp \mathbf{e}_z$. The precession angle is defined by the ratio of this two components of the field via $\tan \vartheta = \hat{H}_\perp / \hat{H}_\parallel$. The external fields reported are those in the ferrofluid film far away from the clusters. In fig. 2 we show the stability of such

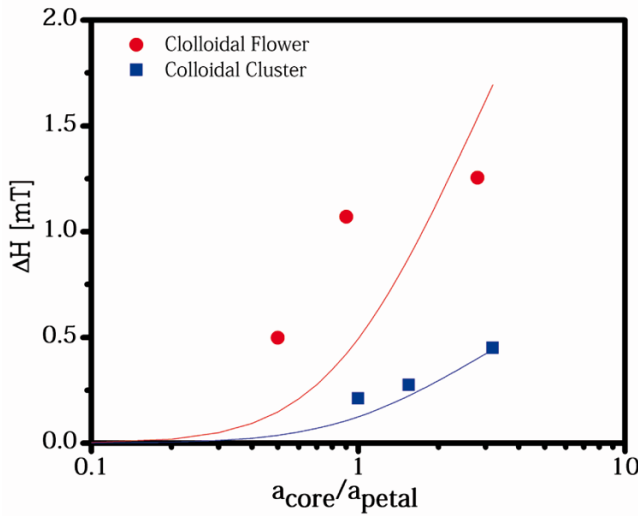


Fig. 3. (Colour on-line) Dependence of the width of the hysteresis loop of the formation and rupture of colloidal flowers (red) and diamagnetic clusters (blue) on the ratio of the core radius and the petal radius. The red and blue lines are fits according to eq. (8).

clusters as we sweep the normal component \hat{H}_\perp of the precessing field. Colloidal flowers are stable for low precession angles (large normal field \hat{H}_\perp) while clusters of holes are stable at large precession angles (small normal field \hat{H}_\perp). Decreasing the normal component of the field destabilizes the colloidal flowers and they fall apart at a critical field $\hat{H}_{\perp c1}$. If we start the experiment at $\hat{H}_\perp = 0$ one observes a mixture of magnetic hole clusters and paramagnetic beads. Colloidal flowers form from this mixture upon surmounting a second threshold $\hat{H}_{\perp c2} > \hat{H}_{\perp c1}$. We characterize the width of this hysteresis by the difference of the two critical fields $\Delta\hat{H}_\perp = \hat{H}_{\perp c2} - \hat{H}_{\perp c1}$. The width of the hysteresis $\Delta\hat{H}_\perp$ is a measure of how strongly the transition is of first order.

A similar hysteresis is measured when disassembling diamagnetic clusters by increasing the normal component \hat{H}_\perp of the precessing field and reassembling a cluster of a generically different shape and size when decreasing the field. The strength of the transition both for the colloidal flowers as well as for the magnetic hole clusters depends on the size ratio a_1/a_2 of the colloids of the core and of the petals. In fig. 3 we plot the width of the hysteresis $\Delta\hat{H}_\perp$ versus the size ratio a_1/a_2 . The width of the hysteresis increases with the size ratio.

The rotating parallel component and the contrast of the imaginary part of the magnetic susceptibility $\Delta\chi''$ of the cluster to the surrounding ferrofluid result in a torque

$$\tau = 4\pi\mu_0\Delta\chi''V\hat{H}^2\sin^2\vartheta.$$

Here μ_0 is the vacuum permeability, V denotes the volume of the cluster, and \hat{H} is the absolute value of the magnetic field. This torque causes the clusters to rotate around their core with an angular frequency $\omega < \Omega$. The ratio

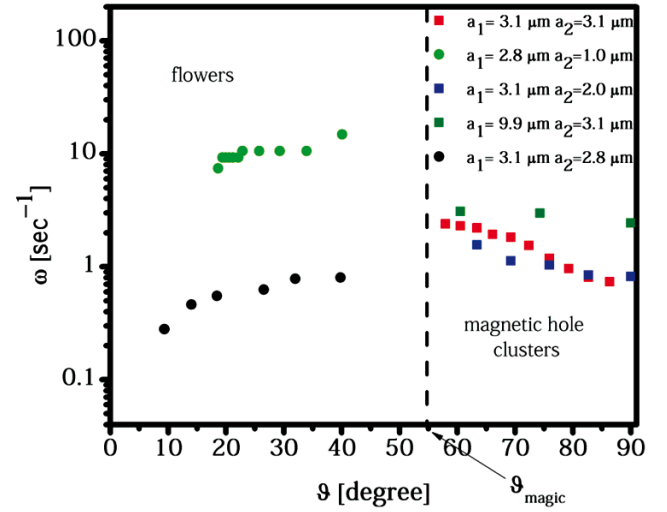


Fig. 4. The angular velocity of different colloidal flowers and diamagnetic clusters as a function of the precession angle recorded at a constant in-plane rotating field of $\hat{H}_\parallel = 1.62$ mT at a constant precession angular frequency of $\Omega = 188$ s $^{-1}$.

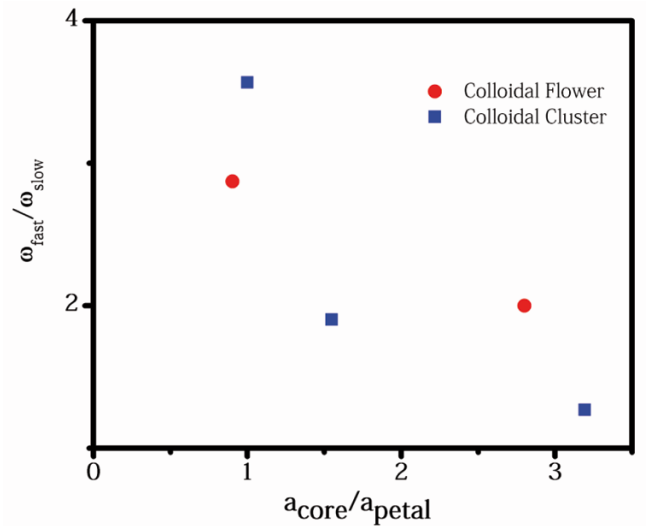


Fig. 5. The angular velocity ratio of different colloidal flowers and diamagnetic clusters near and far from the magic angle as a function of the ratio of the core to the petal radii.

$\omega/\hat{H}^2\sin^2\vartheta$ measures how efficient the magnetic field rotation is converted into a rotation of the cluster. In fig. 4 we plot the angular frequency ω at fixed in-plane field strength and frequency as a function of the precession angle ϑ for different clusters. Some of the clusters show a speeding up when one approaches the magic angle [13], where the clusters fall apart. Other clusters do not change their angular frequency when changing the normal component of the field. We characterize the cluster speed up by the ratio $\omega_{\text{fast}}/\omega_{\text{slow}}$, where ω_{fast} denotes the angular frequency just before rupture and ω_{slow} is the angular frequency at low (high) precession angle where the colloidal flower (magnetic hole cluster) is stable.

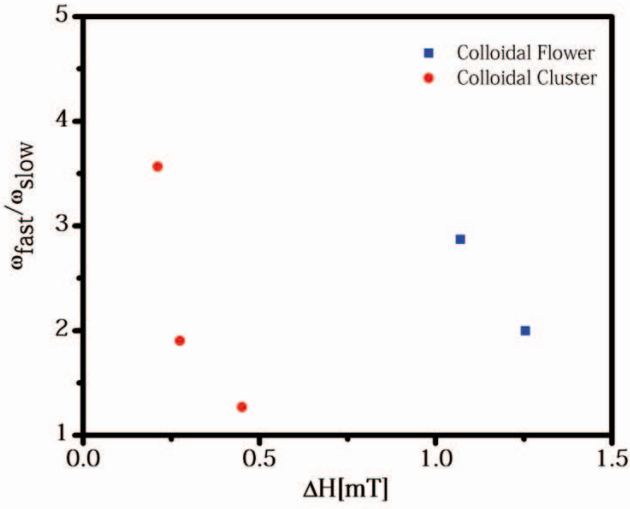


Fig. 6. The angular velocity ratio of different colloidal flowers and diamagnetic clusters near and far from the magic angle as a function of width of the hysteresis.

In fig. 5 we plot the cluster speed up *versus* the size ratio a_1/a_2 of the colloids of the core and of the petals. The speed up decreases with the size ratio for both the colloidal flowers and for the magnetic hole clusters.

Figures 3 and 5 show that both the width of the hystereses and the speed up of the rotation correlate with the ratio of the core-to-the-petal radius $a_{\text{core}}/a_{\text{petal}}$. We may combine figs. 3 and 5 to measure the speed up as a function of the strength of the first order transition. Hence, in fig. 6 we plot the cluster speed up *versus* the width of the hysteresis. A large speed up is observed for small hysteresis while no speed up occurs at large hysteresis.

4 Discussion

If we consider the core particle to be larger than the particles in the ring it is a good approximation to describe the local magnetic field as that in the absence of the petal particles. Toussaint *et al.* [14] have shown that image dipoles due to the presence of the ferrofluid glass walls can cause a first-order transition with two stable distances between the diamagnets. Here those effects are neglected since the sample thickness is much larger than the separation of the petals from the core. Neglecting the image dipoles, the field from the core is described by

$$\mathbf{H} = \begin{cases} \left[\mathbf{I} + \frac{a_1^3(\chi_c - \chi_F)}{1 + \chi_c + 2(1 + \chi_F)} \frac{3\mathbf{r}\mathbf{r} - r^2\mathbf{I}}{r^5} \right] \cdot \mathbf{H}_{\text{ext}}, & \text{for } r > a_1, \\ \frac{3(1 + \chi_F)}{1 + \chi_c + 2(1 + \chi_F)} \mathbf{H}_{\text{ext}}, & \text{for } r < a_1, \end{cases} \quad (1)$$

where \mathbf{I} denotes the unit tensor, and χ_c denotes the susceptibility of the core particle of radius a_1 . The effective magnetic moment of the core and petal particles $\mathbf{m}_c = V_c(\chi_c - \chi_F)\mathbf{H}(r = 0)$ and $\mathbf{m}_P = V_P(\chi_P - \chi_F)\mathbf{H}(r = a_1 + r_2)$ are thus determined by the local field at the particle positions $r = 0$ and $r = a_1 + r_2$, the volumes V_c and

V_P of the particles and the susceptibility contrasts to the ferrofluid. The dipolar interaction hence reads

$$\begin{aligned} W &= -\frac{\mu_0}{4\pi} \mathbf{m}_c \cdot \left[\frac{3\mathbf{r}\mathbf{r} - r^2\mathbf{I}}{r^5} \right] \cdot \mathbf{m}_P \\ &= -\gamma \mathbf{H}_{\text{ext}} \cdot \left[\frac{3\mathbf{r}\mathbf{r} - r^2\mathbf{I}}{r^5} + \frac{a_1^3(\chi_c - \chi_F)}{1 + \chi_c + 2(1 + \chi_F)} \right. \\ &\quad \left. \times \left(\frac{3\mathbf{r}\mathbf{r} - r^2\mathbf{I}}{r^5} \right)^2 \right] \cdot \mathbf{H}_{\text{ext}}, \end{aligned} \quad (2)$$

where

$$\gamma = \frac{\mu_0}{4\pi} V_P V_c \frac{3(1 + \chi_F)}{1 + \chi_c + 2(1 + \chi_F)} (\chi_c - \chi_F)(\chi_P - \chi_F) \quad (4)$$

and \mathbf{r} is the separation vector between the core and petal particle. The first term in (3) corresponds to the interaction of the petal particle in the unperturbed external field and the second term is the perturbation of the magnetic moment of the petal particle due to the presence of the core particle. For an external field $\mathbf{H}_{\text{ext}} = H_{\text{ext}}(\sin \vartheta_{\text{ext}}[\mathbf{e}_x \cos \Omega t + \mathbf{e}_y \sin \Omega t] + \cos \vartheta_{\text{ext}} \mathbf{e}_z)$ and a petal particle sitting in the equatorial plane at a distance $r = a_1 + r_2$ the time-averaged dipole interaction energy reads

$$\begin{aligned} \overline{W} &= \frac{1}{2} \frac{\gamma H_{\text{ext}}^2}{(a_1 + r_2)^3} \left(1 + \frac{\beta}{(1 + r_2/a_1)^3} \right) \\ &\quad \times \left[P_2(\cos \vartheta_{\text{ext}}) - \frac{4\beta}{\beta + (1 + r_2/a_1)^3} \right], \end{aligned} \quad (5)$$

where

$$\beta = \frac{(\chi_c - \chi_F)}{1 + \chi_c + 2(1 + \chi_F)}. \quad (6)$$

The first term in (5) corresponds to a renormalized long-range dipole interaction that scales with second Legendre polynomial $P_2(\cos \vartheta_{\text{ext}})$ of the precession angle ϑ_{ext} and switches sign when passing the magic angle. This part of the interaction is attractive if $(\chi_c - \chi_F)(\chi_P - \chi_F)P_2(\cos \vartheta_{\text{ext}}) < 0$ and explains the stability of the colloidal flowers ($\chi_c - \chi_F > 0, \chi_P - \chi_F < 0, P_2(\cos \vartheta_{\text{ext}}) > 0$) for small precession angles $\vartheta_{\text{ext}} < \vartheta_{\text{magic}}$ and the stability of the diamagnetic clusters ($\chi_c - \chi_F < 0, \chi_P - \chi_F < 0, P_2(\cos \vartheta_{\text{ext}}) < 0$) for large precession angles $\vartheta_{\text{ext}} > \vartheta_{\text{magic}}$. The second term is independent of the precession angle. Its sign does not depend on the sign of the susceptibility contrast $\text{sign}(\chi_c - \chi_F)$ of the core particle to the ferrofluid. The second term is repulsive for petal particles that are magnetic holes ($\chi_P - \chi_F < 0$), while for paramagnetic particles it is attractive. The destabilizing correction term is short range. This results in an equilibrium distance of the petal from the core given by

$$r_{2,\text{min}} = a_1 \left[\sqrt[3]{\frac{4\beta}{P_2(\cos \vartheta_{\text{ext}})} - \beta - 1} \right], \quad (7)$$

that moves from infinity at the magic angle $\vartheta_{\text{ext}} = \vartheta_{\text{magic}}$ toward the hard-core distance a_2 as one moves away from

the magic angle. The picture changes when the dipole interactions between the petals are taken into account as well. Here the different range of both interactions becomes important when summing up the interaction of all petal particles. We expect that in a cluster of N particles that the dipole interaction increases with the number of pairs of particles that scales as N^2 , while the short-range correction increases with the number of nearest neighbor particles that scales like N . This explains the hystereses since once a cluster is formed it can be stabilized by the long-range dipole interactions even when a single pair of particles is not yet stable. The minimum radius of N petals will hence be different from that of one petal described by eq. (7). We expect the hystereses to roughly scale with the ratio of the long-range to short-range interactions such that

$$\Delta H \propto 1/(\beta + (1 + a_2/a_1)^3). \quad (8)$$

In fig. 3 we have incorporated curves according to eq. (8) with the prefactor of eq. (8) fitted to the data. The fit agrees well for the colloidal cluster but is less accurate for the colloidal flowers. This is not too surprising since the different susceptibility of the core of the flower adds to the complexity of the phenomenon. The width of the hystereses is a measure for the strength of the first-order transitions. If the transition is weakly first order, some of the second-order critical phenomena are likely to persist. This is what we observe in the critical speeding up. For a second-order transition we would expect the rotation speed of the cluster to diverge. For a weakly first-order transition there is significant increase when approaching the transition, while no significant increase is observed when the transition is strongly first order. The interaction between particles at the magic angle in an isotropic environment vanishes. Some interaction will persist if the larger size of the core renders the environment anisotropic. The self-consistent deviation of the system from isotropic is what stabilizes or destabilizes the particular conformation and renders the transition from second to first order. It is therefore conceivable that the presence of a large core particle is responsible for the strong first-order type of transitions in the clusters with a large core. The corresponding second-order speeding up of the rotation of the cluster is destroyed by the large core and partially persists for smaller core sizes.

5 Conclusions

The rotation of colloidal clusters of non-magnetic holes and of mixtures of paramagnetic beads with non-magnetic

holes in a ferrofluid in a precessing external magnetic field depends on the precession angle of the external field that serves as a control parameter for the stability of the clusters. Near the magic angle cluster-shape-dependent depolarization fields cause an orientation of the local field deviating from the external field and render cluster transitions weakly or strongly first order. If the transition is weakly first order a critical speeding up of the cluster rotation is observed. No speeding up occurs for strongly first-order cluster transitions with hysteresis. The strength of the first-order transition is larger the larger the size of the core as compared to the petal particles of the cluster.

This work is supported by the German Science Foundation within the cluster of excellence SFB840.

Open Access This is an open access article distributed under the terms of the Creative Commons Attribution License (<http://creativecommons.org/licenses/by/2.0>), which permits unrestricted use, distribution, and reproduction in any medium, provided the original work is properly cited.

References

1. P. Pieranski, *Contemp. Phys.* **24**, 25 (1983).
2. A. vanBlaaderen, R. Ruel, P. Wiltzius, *Nature* **385**, 321 (1997).
3. James E. Martin, Eugene Venturini, Gerald L. Gulley, Jonathan Williamson, *Phys. Rev. E* **69**, 021508 (2004).
4. N. Casic, S. Schreiber, P. Tierno, W. Zimmermann, Th.M. Fischer, *EPL* **90**, 58001 (2010).
5. A.P. Gast, C.F. Zukoski, *Adv. Colloid Interface Sci.* **30**, 153 (1989).
6. N. Osterman, I. Poberaj, J. Dobnikar, D. Frenkel, P. Zihlerl, D. Babic, *Phys. Rev. Lett.* **103**, 228301 (2009).
7. G. Helgesen, P.O. Pieranski, A.T. Skjeltorp, *Phys. Rev. A* **42**, 7271 (1990).
8. E.R. Andrew, A. Bradbury, R.G. Eades, *Nature* **182**, 1659 (1958).
9. J. Cernak, G. Helgesen, A.T. Skjeltorp, *Phys. Rev. E* **70**, 031504 (2004).
10. R.M. Erb, H.S. Son, B. Samanta, V.M. Rotello, B.B. Yellen, *Nature* **457**, 999 (2009).
11. K.H. Li, B.B. Yellen, *Appl. Phys. Lett.* **97**, 083105 (2010).
12. A. Ray, S. Aliaskarisohi, Th.M. Fischer, *Phys. Rev. E* **82**, 031406 (2010).
13. P. Tierno, R.M. Muruganathan, Th.M. Fischer, *Phys. Rev. Lett.* **98**, 028301 (2007).
14. R. Toussaint, J. Akselvoll, G. Helgesen, A.T. Skjeltorp, *Phys. Rev. E* **69**, 011407 (2004).

Chapter 5

Magnetic field controlled
composite

paramagnetic-diamagnetic
colloidal phases

**Magnetic field controlled composite paramagnetic-diamagnetic
colloidal phases**

A. Ray, and Th. M. Fischer,

Submitted to The Journal of Physical Chemistry B

Magnetic field controlled composite paramagnetic-diamagnetic colloidal phases

A. Ray, and Th. M. Fischer[†]

Institut für Experimentalphysik, Universität Bayreuth, 95440 Bayreuth, Germany.

Abstract

We report on differently ordered colloidal phases of a mixture of paramagnetic and diamagnetic colloids subject to a quickly varying time dependent magnetic field. Effectively paramagnetic and effectively diamagnetic colloids are created from paramagnetic and nonmagnetic colloids immersed into a thin film of aqueous ferrofluid. The time averaged dyadic product of the magnetic field with itself serves as a control parameter for a sequence of transitions between differently correlated orientation order between the paramagnetic and diamagnetic colloids. We observe anti- and equimagnetic order along directions that are orthogonal to each other. At the magic angle equimagnetic and antimagnetic directions of the colloidal order change via an intervening biaxial ordered phase to a phase where the equimagnetic ordered direction is replaced by an antimagnetic ordering and vice versa.

1. Introduction

Neutralization of opposite charges is one of the driving concepts leading to the organization of matter on the atomic and molecular scale. The interaction between point charges is isotropic and does not depend on direction. It is spontaneous breaking of rotational symmetry and the quantization of angular momentum that nevertheless produces crystalline structures with directed bonds in atoms and molecules. Colloidal particles have been used as a model for atoms on a larger scale^{1,2}. They however are of mesoscopic size, where quantum phenomena are absent, and angular momentum is a continuous quantity. The principles leading to directed bonds in microscopic systems therefore do not work on the colloidal scale. In isotropically interacting colloids steric interactions are the means to spontaneously break rotation symmetry and form a colloidal crystal³. The only possibility of obtaining directed bonds in colloidal systems is by using colloidal particles that are intrinsically anisotropic. For this reason chemists have synthesized Janus particles^{4,5} and patchy colloids^{6,7} with surface functionalities that vary as a function of the location on the particle surface. Other possibilities are the use of ellipsoidal particles⁸⁻¹⁰ the shape of which is different in different directions. A third possibility is to use a magnetic¹¹ or electric¹² dipole moment using an external magnetic or electric field. Induced paramagnetic dipoles do not neutralize in an external field but build up an induced magnetization with a macroscopic magnetic moment given by the magnetization of the sample times its volume. The situation changes when considering a mixture of paramagnetic and diamagnetic colloids¹³. Diamagnets and paramagnets point into opposite directions in the same field. They are able to *neutralize* each other on a macroscopic scale. In this sense, mixtures of paramagnets and diamagnets in an external magnetic field are a model system for neutralizing, anisotropically interacting particles that possess a variety of mesoscopic arrangements that is richer than that of isotropic colloids and than that of non-neutralizing anisotropic colloids. In the current manuscript, we show a few of the most obvious colloidal phases that form in such a system, when we apply a field varying on time-scales faster than the

inter particle dynamics.

2. Experiment

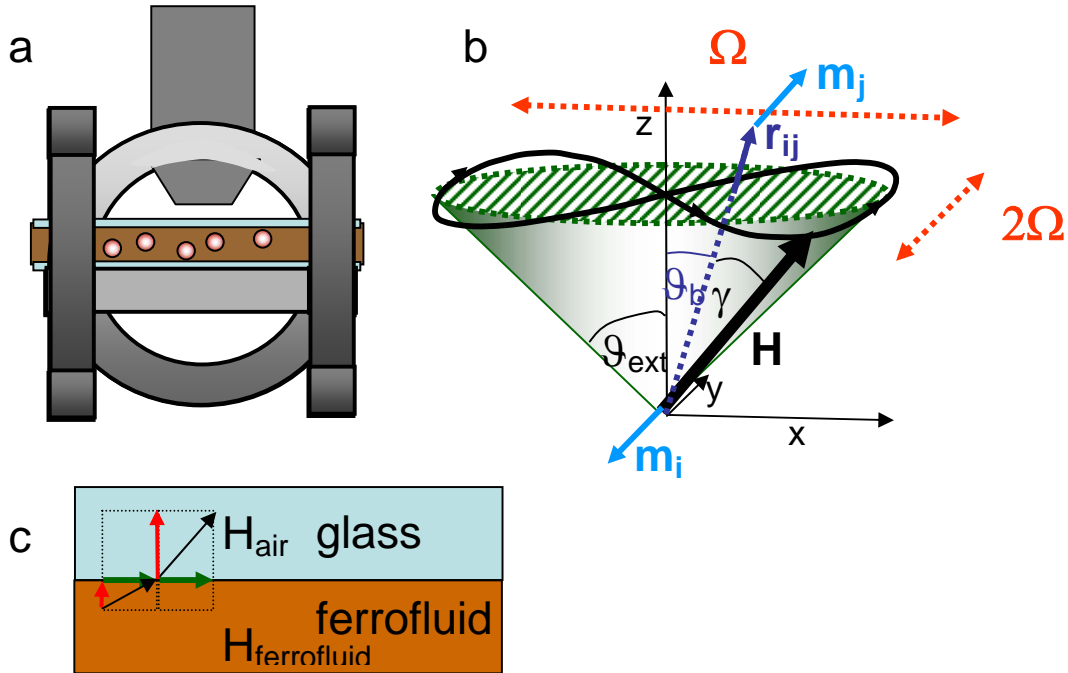


Figure 1 a) Scheme of the experimental setup. b) Scheme of the field modulation The field varies in time according to $\mathbf{H}(t) = \hat{H} \cos \vartheta_{ext} \mathbf{e}_z + \hat{H} \sin \vartheta_{ext} [\mathbf{e}_x \sin \Omega t + \mathbf{e}_y \sin 2\Omega t]$ with the tip of the magnetic field vector following the black Lissajou figure. This modulation produces the same time averaged dipole interactions as a field precessing at a precession angle of ϑ_{ext} around the z-axis (green cone) but causes no net torque on the colloidal assembly. $\gamma(t)$ denotes the angle between the particle separation vector \mathbf{r}_{ij} and the field. Only the projection angles of the field ϑ_{ext} and the bond ϑ_b enter in the angular dependence of the time averaged interaction. Whether the interaction between the induced moments \mathbf{m}_i and \mathbf{m}_j is attractive or repulsive depends on whether ϑ_{ext} and ϑ_b are smaller and larger than the magic angle. The interaction also is proportional to the

product of the effective susceptibilities of the pair of particles. In the scheme a diamagnetic particle sits at the origin and a paramagnetic particle at \mathbf{r}_{ij} . The magnetic moment \mathbf{m}_i of the diamagnet is pointing opposite to the field, while \mathbf{m}_j points along the magnetic field. c) The magnetic field is generated by coils outside the ferrofluid. At the ferrofluid glass interface the magnetic boundary conditions (continuity of H_{\perp} and B_{\parallel}) cause a deflection of the field. All field directions mentioned in this work are expressed in terms of their value inside the ferrofluid.

In our experiment we have used micron-sized superparamagnetic particles of diameter 2.8 μm (Invitrogen Dynal Oslo, Norway), fluorescence red polystyrene particles of diameter 1.0 μm (Thermo Scientific) and water based ferrofluid EMG 707 FerroTec Ferrosound (FerroTec GmbH, Germany) of susceptibility $\chi_f=1.5$. Both the superparamagnetic and fluorescence polystyrene particles were immersed in undiluted ferrofluid with controlled proportions and were placed between two cover slips. The sandwiched cover slips were placed in a time dependent magnetic field produced by 5 coils (two coils for the x direction, 2 coils for the y direction in the plane of the ferrofluid film and one z-coil normal to the film) and observed with either reflection or fluorescence microscopy (LEICA DM5000, Leica Microsystems Wetzlar GmbH, Germany).

Typical fluxes in one direction were of the order of 3 mT and orientational fluctuations of the magnetic field were of the order of $f = \Omega/2\pi = 10\text{-}40$ Hz. At these conditions the viscous forces inhibit the motion of individual particles into their instantaneous equilibrium positions and only the time averaged dipolar interactions between the particles force them into their time averaged equilibrium conformation. The field direction of the magnetic field changes from the air into the ferrofluid film according to $\hat{H}_{\perp}^{\text{ferrofluid}} = \hat{H}_{\perp}^{\text{air}} / (1 + \chi_F)$ and $\hat{H}_{\parallel}^{\text{ferrofluid}} = \hat{H}_{\parallel}^{\text{air}}$, and the orientation angle in the ferrofluid and in the air are related via $\tan \vartheta^{\text{ferrofluid}} = (1 + \chi_F) \tan \vartheta^{\text{air}}$. χ_F denotes the magnetic susceptibility of the ferrofluid. All external fields and external orientations are given in terms of their values inside the ferrofluid.

2. time averaged dipole interactions

The magnetic field induces excess magnetic moments $\mathbf{m}_i(t)$ in the particles that interact via the dipole dipole interaction

$$W_{ij} = -\frac{\mu_0}{4\pi} \mathbf{m}_i(t) \mathbf{m}_j(t) : \frac{3\mathbf{r}_{ij}\mathbf{r}_{ij} - r_{ij}^2\mathbf{I}}{r_{ij}^5} \quad (1)$$

, where μ_0 denotes the vacuum permeability, \mathbf{r}_{ij} the separation vector between the interacting beads and \mathbf{I} denotes the unit tensor. The tensor $\frac{3\mathbf{r}_{ij}\mathbf{r}_{ij} - r_{ij}^2\mathbf{I}}{r_{ij}^5}$ is traceless and

hence only the traceless part $\mathbf{m}_i\mathbf{m}_j - \frac{1}{3}(\mathbf{m}_i \cdot \mathbf{m}_j)\mathbf{I}$ of the tensor $\mathbf{m}_i\mathbf{m}_j$ is relevant for the interaction between the beads. If we neglect the influence of other beads on the excess magnetic moment of an individual bead, and if we assume an instantaneous response of the bead magnetization then the magnetic moment is related to the external field via

$$\mathbf{m}_i = \Delta\chi_{eff}^i V_i \mathbf{H}_{ext} \quad (2)$$

where

$$\Delta\chi_{eff}^i = \frac{3(1 + \chi_F)(\chi_i - \chi_F)}{1 + \chi_i + 2(1 + \chi_F)} \quad (3)$$

is the effective susceptibility contrast with χ_f and χ_i the ferrofluid and particle susceptibility and V_i the particle volume. The dipole interaction can therefore be rewritten as:

$$W_{ij} = -\frac{\mu_0 \Delta\chi_{eff}^i \Delta\chi_{eff}^j V_i V_j}{4\pi} \frac{3\mathbf{r}_{ij}\mathbf{r}_{ij} - r_{ij}^2\mathbf{I}}{r_{ij}^5} : \left[\mathbf{H}_{ext}(t) \mathbf{H}_{ext}(t) - H_{ext}^2(t) \frac{\mathbf{I}}{3} \right] \quad (4)$$

Since in our experiments the intra particle dynamics is slow compared to the modulation of the external field the particle separations can be considered time independent during one period of the magnetic field such that the time average taken over one period

affects only the traceless magnetic field tensor $\mathbf{H}_{ext}(t)\mathbf{H}_{ext}(t) - H_{ext}^2(t)\frac{\mathbf{I}}{3}$. For a modulation of the form

$$\mathbf{H}(t) = \hat{H}_z \mathbf{e}_z + \hat{H}_x \mathbf{e}_x \sin \Omega t + \hat{H}_y \mathbf{e}_y \sin 2\Omega t \quad (5)$$

the time averaged traceless dyadic product of the external field is diagonal in x,y,z coordinates and reads:

$$\overline{\mathbf{H}_{ext}(t)\mathbf{H}_{ext}(t) - H_{ext}^2(t)\frac{\mathbf{I}}{3}} = -\frac{\hat{H}_{ext}^2}{3} P_2(\cos \mathcal{G}_{ext}) \begin{pmatrix} 1 & & \\ & 1 & \\ & & -2 \end{pmatrix} + \frac{\varepsilon \hat{H}_{ext}^2}{3} P_2^2(\cos \mathcal{G}_{ext}) \begin{pmatrix} 1 & & \\ & -1 & \\ & & 0 \end{pmatrix} \quad (6)$$

where $\hat{H}_{ext} = \sqrt{(\hat{H}_x^2 + \hat{H}_y^2)/2 + \hat{H}_z^2}$, $\sin \mathcal{G}_{ext} = \frac{\hat{H}_z}{\hat{H}_{ext}}$ is the time averaged precession angle

and $\varepsilon = \frac{\hat{H}_x^2 - \hat{H}_y^2}{2\hat{H}_{ext}^2}$ is the eccentricity of the modulation. Insertion of equation (6) into (4)

leads to the time averaged dipolar interaction in the form:

$$\overline{W}_{ij} = -\frac{\mu_0}{4\pi} \frac{\Delta\chi_{eff}^i V_i \Delta\chi_{eff}^j V_j H_{ext}^2}{(r_{ij})^3} \left[P_2(\cos \mathcal{G}_{ext}) P_2(\cos \mathcal{G}_b) + \varepsilon P_2^2(\cos \mathcal{G}_{ext}) P_2^2(\cos \mathcal{G}_b) \cos(2\varphi_b) \right] \quad (7)$$

where \mathcal{G}_b and φ_b are the bond tilt and azimuth angle defined via $\sin \mathcal{G}_b = \frac{z}{r}$ and

$\sin \varphi_b = \frac{y}{r \cos \mathcal{G}_b}$ and P_2 and P_2^2 are Legendre polynomials of degree 2 and associated

Legendre polynomials of degree 2 and order 2. For vanishing eccentricity of the modulation the averaged dipole interaction is purely uniaxial and the interaction only depends on the bond tilt angle. The averaged dipole interaction changes sign at the magic angle $\mathcal{G}_b = \mathcal{G}_{magic}$ i. e. the zero of the second Legendre polynomial. In magic angle spinning NMR this magic angle \mathcal{G}_{magic} is used to suppress the influence of dipole interactions on NMR line shapes. Here it is used in a similar way to switch the sign of the average dipole dipole interactions. From equation (6) we deduce that there are three

ways to switch the sign. The product of the effective susceptibility contrasts $\Delta\chi_{eff}^i \Delta\chi_{eff}^j$ is positive for similar beads but negative for a paramagnetic and diamagnetic pair of beads. Bond angles that are attractive for similar beads are repulsive for a paramagnetic and diamagnetic pair of beads and vice versa. We might switch the sign by using precession angles of the magnetic field $\mathcal{G}_{ext} > \mathcal{G}_{magic}$ below and above the magic angle. Finally the interaction switches sign when the bond tilt angle between the beads is $\varphi_b > \mathcal{G}_{magic}$ below and above the magic angle.

With eccentricity the bond structure becomes biaxial. The biaxiality is of minor importance if the precession angle of the field is far away from magic, since then the uniaxial components overpower the biaxiality. Close to the magic angle, however, the eigenvalue structure of the dyadic product of the magnetic field changes such that one eigenvalue is zero while the other two have opposite sign. This results in one attractive one repulsive and one indifferent bond direction.

In figure 2 we plot the color coded bond angular dependence of the averaged dipole interaction for similar beads for an eccentricity of 10% when passing through the magic precession angle. Far away from the magic precession angle (a) the cyan color at the latitude of the magic bond tilt angle separates the attractive polar bond directions (blue-violet) from the repulsive directions around the equator. When approaching the magic precession angle (b) the indifferent (cyan) zone approaches the equator near $\varphi_b = 0, \pi$ and remains near the magic bond tilt angle for intermediate longitudes. The indifferent zone from the southern and northern hemisphere eventually merge (c) when the eigenvalue in x direction switches sign restricting the repulsive directions around the equator to the longitudes around $\varphi_b = \pm\pi/2$. When further approaching the magic precession angle the merged indifferent zones disjoin into a eastern and western zone creating an attractive plane along $\varphi_b = 0, \pi$ (d). Then the indifferent zone moves toward the poles near the longitudes around $\varphi_b = \pm\pi/2$, where they merge right at the magic precession angle (e). It is at the magic precession angle where the eigenvalue in z-direction switches sign, leaving an attractive direction along the x-axis and a repulsive

direction along the y-axis. When passing the magic precession angle the indifferent zones disjoin and retreat along $\varphi_b = 0, \pi$ (f). The plane $\varphi_b = \pm\pi/2$ is now repulsive. Finally the indifferent zones merge at the equator near $\varphi_b = \pm\pi/2$ the third eigenvalue along the y axis switches sign (g) and the indifferent zone disjoin to move back (h) to the magic bond tilt angle with a polar repulsive direction and an equatorial attractive direction that is just opposite to the behavior observed for a precession angle below magic (i). The effect of the eccentricity is hence a sequential change of sign of the three eigenvalues instead of a simultaneous switch for a truly uniaxial modulation. Note that the same result holds for a paramagnetic and a diamagnetic bead when we interchange attractive and repulsive.

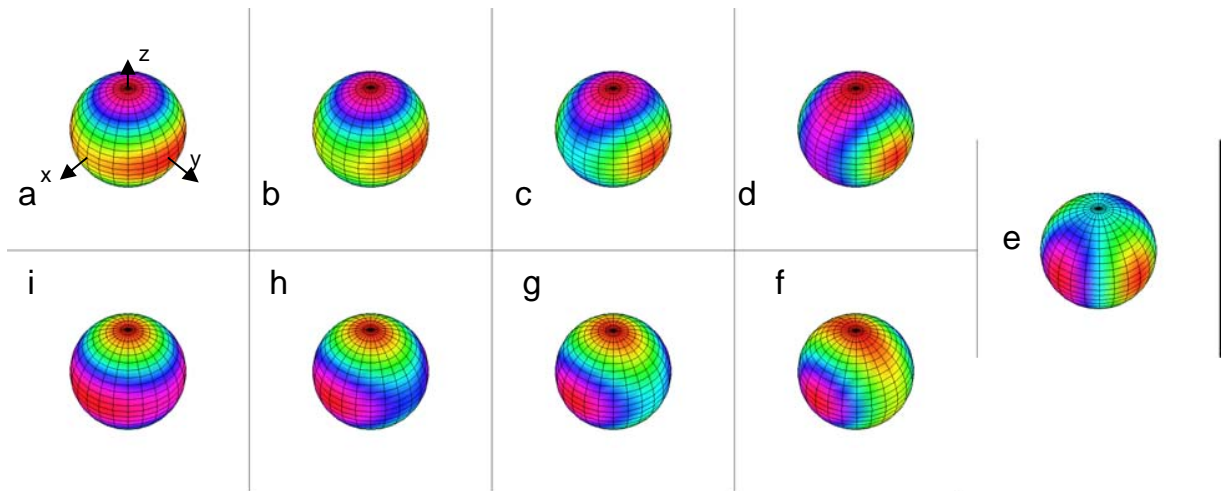


Figure 2) *angular dependence of the time averaged dipolar interactions color coded from (violet = attractive via cyan = indifferent toward orange = repulsive) for precession angles a)-d) $\vartheta_{ext} < \vartheta_{magic}$ e) $\vartheta_{ext} = \vartheta_{magic}$ and f)-i) $\vartheta_{ext} > \vartheta_{magic}$ and an eccentricity of 10%. The eigenvalues switch sign in figure c) for the x-direction, in e) for the z-direction and in g) for the y-direction*

It is therefore clear that the use of time dependent magnetic fields varying in all three directions of space open up the possibility to create a rich variety of differently arranged assemblies of colloids. The use of paramagnets and diamagnets further enriches the possibilities since bond directions between magnetically similar and different particles

point along directions that are orthogonal to each other. Some of those assemblies are shown in the next section.

3. Results

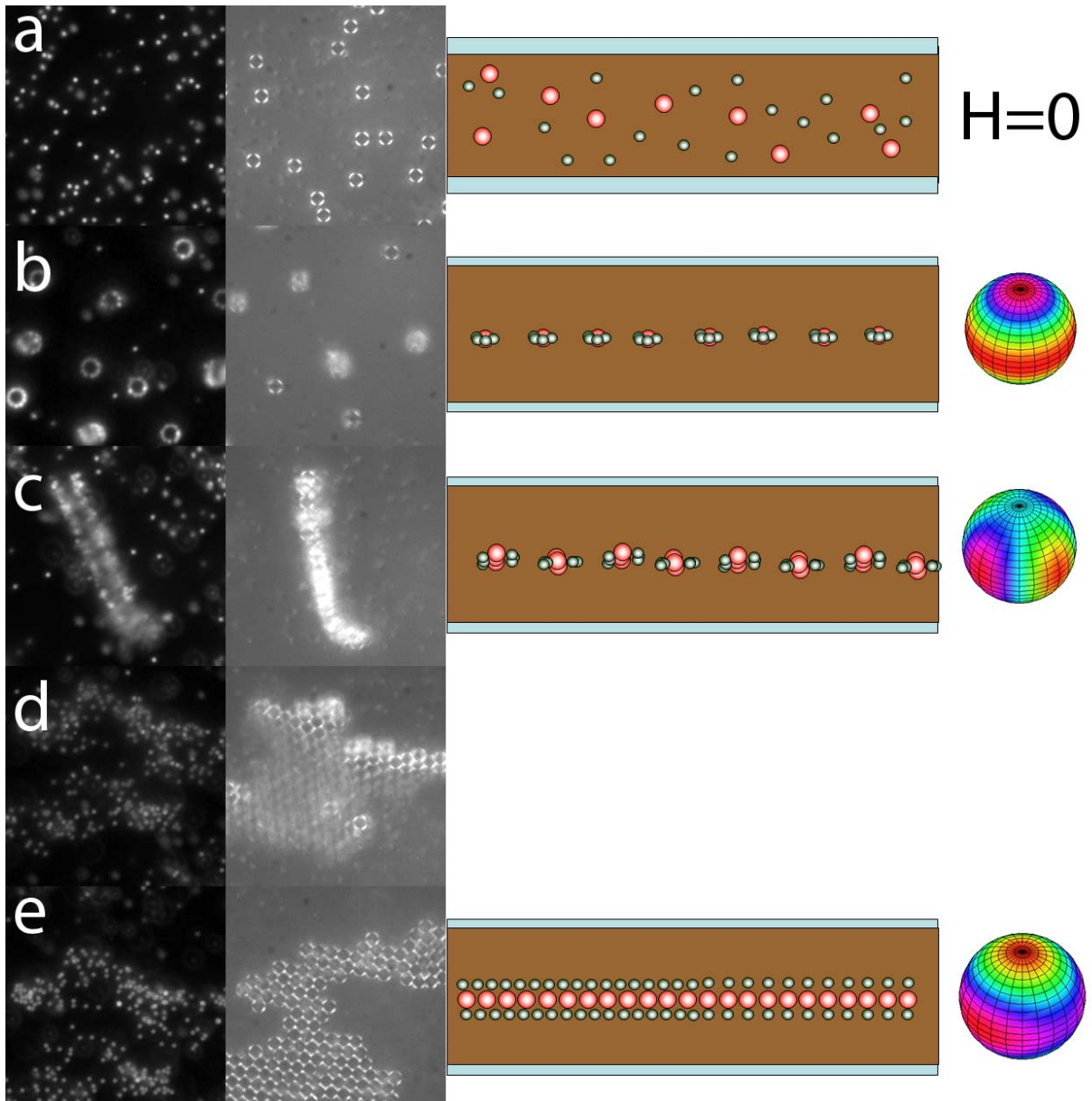


Figure 3: collection of fluorescence- (left) and polarization reflection microscope images (middle left) together with a side view scheme of the structure (middle right) of a mixture of paramagnetic beads $2a_p=2.8\mu\text{m}$, and effective diamagnets $2a_d=1.0\mu\text{m}$ immersed into a undiluted aqueous ferrofluid $\chi_f=1.5$. Fluorescence microscopy images visualize the

diamagnets while polarization reflection microscopy images visualize the paramagnets. The right figure shows the corresponding angular dependence of the dipole interactions as explained in figure 2. The images in figure a) show the random arrangement in the absence of a magnetic field. Figures b-d are recorded in a magnetic field of $H_{\parallel} = (\hat{H}_x^2 + \hat{H}_y^2)/2 = 1.82\text{mT}$ and a frequency $\Omega = 120\text{s}^{-1}$. The vertical field (precession angle) in the images were b) $H_z^{\text{air}} = 26.5\text{mT}$ ($\vartheta_{\text{ext}} = 10^\circ$) c) $H_z^{\text{air}} = 4.0\text{mT}$ ($\vartheta_{\text{ext}} = 49^\circ$) d) $H_z^{\text{air}} = 2.22\text{mT}$ ($\vartheta_{\text{ext}} = 64^\circ$) e) $H_z^{\text{air}} = 1.27\text{mT}$ ($\vartheta_{\text{ext}} = 75^\circ$).

We applied a field of the form equation 5 with an eccentricity of less than 5%. This ensures that the dyadic product of the magnetic field at two different times is a symmetric tensor ($\overline{\mathbf{H}(t)\mathbf{H}(t')} - \mathbf{H}(t')\mathbf{H}(t)} = \mathbf{0}$), where the bar denotes the time average. As a consequence there is no net time averaged torque onto the colloidal structure¹⁴. In what follows we describe the assemblies of paramagnetic and diamagnetic particles as we increase the angle ϑ_{ext} .

Colloidal flowers

In a static field $\hat{H} = 21200\text{ A/m}$, $\vartheta_{\text{ext}} = 0$ normal to the ferrofluid film we observe the formation of colloidal flowers. Such flowers form due to the dipolar attraction of diamagnetic particles in the equatorial plane $\vartheta_b = \pi/2$ of the paramagnets. They have been first discovered by Erb et al.¹³ They are highly dynamic structures where the petals of the flowers may diffuse¹⁵ and they can be easily set into rotation with time dependent magnetic fields having an asymmetric part in the dyadic product¹⁶. Figure 3b shows a fluorescence microscope image of such colloidal flowers with $2a_p = 2.8\mu\text{m}$ paramagnetic cores and $2a_d = 1.0\mu\text{m}$ petals. An ensemble of flowers can be seen via the fluorescent petals of the flower surrounding the non fluorescent paramagnetic cores. The flowers are located in the middle of the sample indicating that gravitation and image dipoles prevent the binding of paramagnetic beads into one dimensional strings with a diamagnetic mantle.

Decorated strings

Upon increasing the precession angle to $\vartheta_{\text{ext}} = 49^\circ$ we observe the formation of paramagnetic strings undulating around the middle plane of the film with a period of three to five beads (figure 3c). The entire structure is decorated with a collection of diamagnets that horizontally adsorb to the undulating string at the sides of the string. The bonds between diamagnets and paramagnets in this structure are also in the horizontal plane but perpendicular to the bonds between the paramagnets in the string. A scheme of the decorated strings is shown to the right of figure 3c. These strings correspond to the biaxial angular dependence of the dipolar interactions.

Sandwiched membranes

At precession angles of the order $\vartheta_{\text{ext}} = 64^\circ$ the paramagnetic beads form membranes instead of strings. These paramagnetic membranes are sandwiched between two layers of diamagnets that adsorb to the membrane on either side. At the transition angle $\vartheta = 51^\circ$ the orientation of the membrane normal is in the plane of the ferrofluid making the sandwich structure clearly visible in the fluorescence microscope image. The two diamagnetic adsorption layers appear as brightly fluorescing lines of diamagnetic beads sandwiching the non fluorescent paramagnets. Upon increasing the precession angle the membrane bends (figure 3d) such that part of the membrane normal remains in the horizontal direction while the normal to the lower part of the membrane now aligns with the film normal. Eventually upon further increasing the precession angle the membrane flattens and entirely lies in the film plane (figure 3e), allowing a closer inspection of the diamagnetic order of the adsorbed layers. For all systems studied here the paramagnetic membrane is a close-packed two dimensional structure with a hexagonal unit cell with unit vectors having the length of a paramagnetic bead diameter $2a_p$. The order of the diamagnetic adsorbate on the contrary varies a lot and sensitively depends on the size of the diamagnetic beads, on the concentration ratio of diamagnets versus paramagnets and on the susceptibility of the diluted background ferrofluid. In what follows we describe the order of the diamagnetic adsorbate under various conditions.

Paramagnetic crystal enslaved diamagnetic gas phase

Figure 3b shows a superposition of a reflection microscopy image of the sample with a fluorescence microscope image of the same sample taken immediately one after another for a tilt angle of $\vartheta_{\text{ext}} = \pi/2$. The paramagnetic particles order into a series of planar clusters surrounded by regions that are completely depleted of paramagnetic colloids. Within the clusters a crystalline hexagonal arrangement of the paramagnetic beads is observed. The arrangement of the diamagnetic colloids is not completely

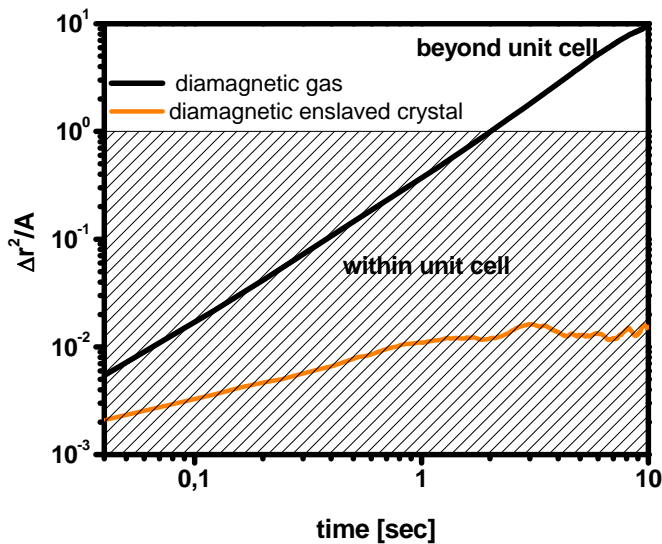


Figure 4: Mean square displacement of the diamagnetic beads upon a cluster for a diamagnetic gas $H_z=0.8\text{mT}$, $\Omega = 120\text{s}^{-1}$, $H_{||}=1.82\text{mT}$, $2a_d=1\mu\text{m}$ (black) and for an enslaved crystal $H_z=1.01\text{mT}$, $\Omega= 120\text{s}^{-1}$, $H_{||}=1.82\text{mT}$, $2a_d=2\mu\text{m}$ (orange). The shaded region corresponds to mean square displacements smaller than the paramagnetic unit cell size.

uncorrelated to the paramagnets. Diamagnetic particles from the paramagnetic depleted regions adsorb on top and below the paramagnetic crystalline clusters. As a result the density of diamagnetic particles on top and below the clusters is larger than the density in the paramagnetic depleted regions. The paramagnetic crystal is sandwiched between

two layers of diamagnetic gas. The diamagnetic particles perform Brownian motion, and the mean square displacement of the diamagnets increases linearly (figure 4) with a slope defining the gaseous diffusion constant of the diamagnets. The increase of the mean square displacement beyond the area of the unit cell of the paramagnetic crystal shows that the diamagnets remain mobile in this phase. For this reason we call this phase the paramagnetic crystal enslaved diamagnetic gas phase. This does not mean that the diamagnetic gas possesses no order. In figure 5 we plot the radial correlation

$$\text{functions } g_{dd}(r)\Delta r = \frac{1}{2N_d^2} \sum_{i,j} \int_r^{r+\Delta r} dr \delta(r - |\mathbf{r}_{id} - \mathbf{r}_{jd}|) \quad \text{and} \quad g_{pp}(r)\Delta r = \frac{1}{2N_p^2} \sum_{i,j} \int_r^{r+\Delta r} dr \delta(r - |\mathbf{r}_{ip} - \mathbf{r}_{jp}|)$$

of the paramagnets and diamagnets, where N_p and N_d are the number of paramagnets and diamagnets in a particular cluster and the \mathbf{r}_{ip} and \mathbf{r}_{jd} are the positions of the i th paramagnet and the j th diamagnet. While the long range behavior of both correlation functions is governed by the shape of the cluster, the short range behavior shows that despite of the mobility of the diamagnetic gas, the crystal order of the paramagnet is imprinted upon the gas via the magnetic field modulations from the paramagnet.

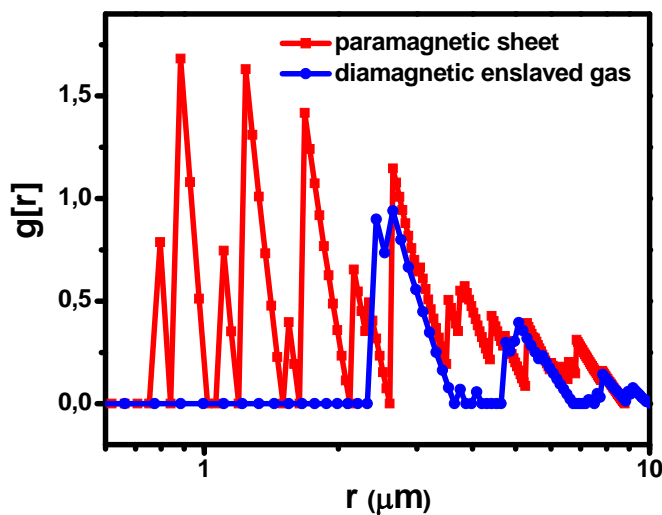


Figure 5 radial correlation function of paramagnetic particles (blue) and diamagnetic particles (red) in a diamagnetic gaseous phase cluster. Although the diamagnetic gas is mobile the crystal structure of the paramagnets is imprinted upon the diamagnets.

The auto-correlation-function of the diamagnets share the peaks occurring in the autocorrelation function of the paramagnets. Since the diameter of the diamagnets is much smaller than that of the paramagnets more than one diamagnet can reside on top and below one paramagnet. We observe a disorder in the occupancy number of the diamagnets of the sites above and below the paramagnetic crystals. A site can be vacant, or have one, two, three or four diamagnets on top of a paramagnet. This disorder is expressed by the substructure in the cross correlation function occurring in the hard core region of the auto correlation function.

Paramagnetic crystal enslaved diamagnetic crystal phase

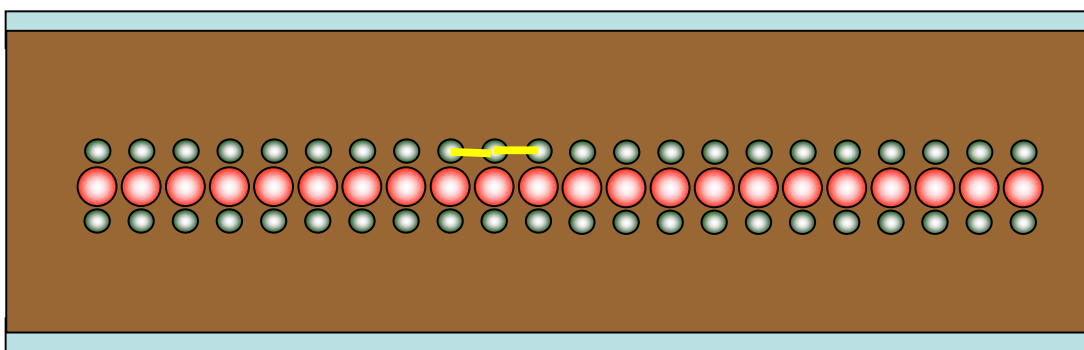
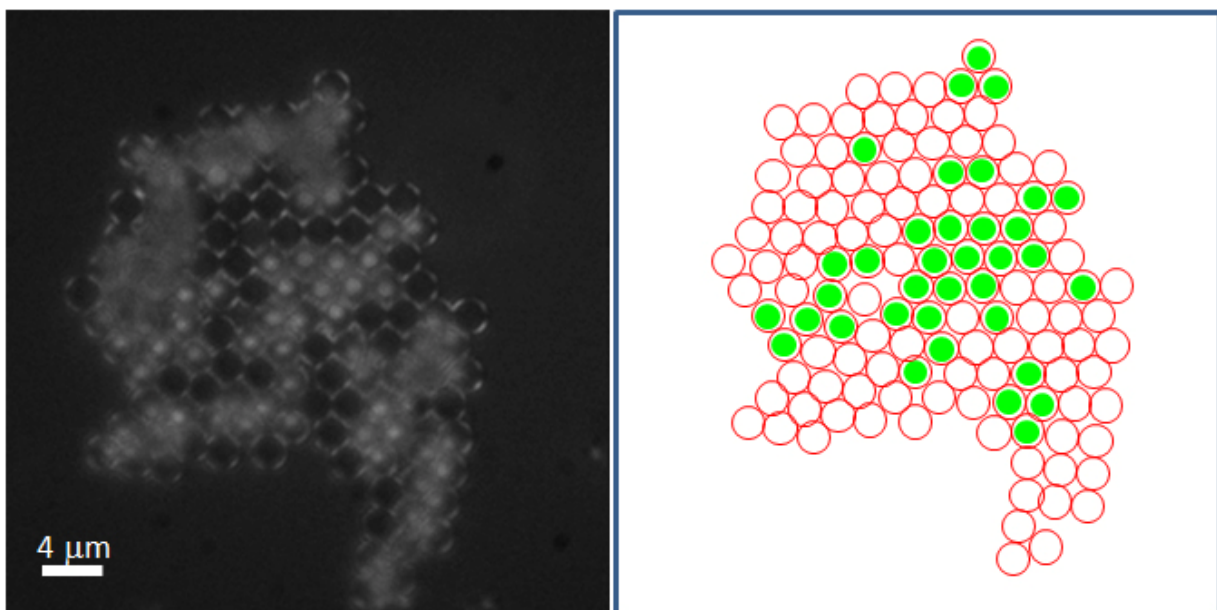


Figure 6 top left) Polarization reflection microscope image of an enslaved crystalline phase of the diamagnets recorded at $H_z=1.01\text{mT}$, $\Omega=120\text{s}^{-1}$, $H_{||}=1.82\text{mT}$, $2a_d=2.0\mu\text{m}$. The magnetic holes are sitting on top of the paramagnets as sketched in the scheme to the top right. The scheme at the bottom shows a side view with two of the frustrated bonds between the diamagnets shown in yellow.

Upon increasing the radii of the diamagnets and upon diluting the ferrofluid we observe a slowing down of the large scale diffusion that eventually stops completely. For a bead diameter $a_d=2.0\mu\text{m}$ the diamagnets remain on top and below the paramagnetic particle they reside. In the plot of the meansquare displacement of the diamagnetic beads in figure 5, we observe a much weaker increase of the mean square displacement with time that eventually settles at roughly 1 percent of the area of a paramagnetic unit cell. According to the Lindemann criterion a crystal should melt when the root mean square displacements of its elements amounts for one tenths of the lattice spacing. We would hence expect a diamagnetic crystal to immediately melt under the current conditions. It is, however, not the interactions between the diamagnets but the interaction with the crystal potential of the paramagnets that causes the crystalline order of the diamagnets. The diamagnets are hence enslaved by the paramagnetic crystal and form two crystal layers growing epitaxial with the same unit cell on the paramagnetic crystals.

Paramagnetic crystal incommensurate diamagnetic crystal phase

For larger densities of the diamagnets and when using concentrated ferrofluids the attraction between the diamagnets overcomes the paramagnetic crystal potential and the diamagnets form close-packed hexagonal crystals on top and below the paramagnetic close-packed hexagonal crystal that has its own unit cell turned by 30 degrees with respect to the paramagnetic unit cell. The close-packed cells of the paramagnetic and diamagnetic crystal layers have periodicities defined by the diameters of the paramagnetic and diamagnetic beads that generically are incommensurate. Figure 7 shows such an incommensurate crystal structure.

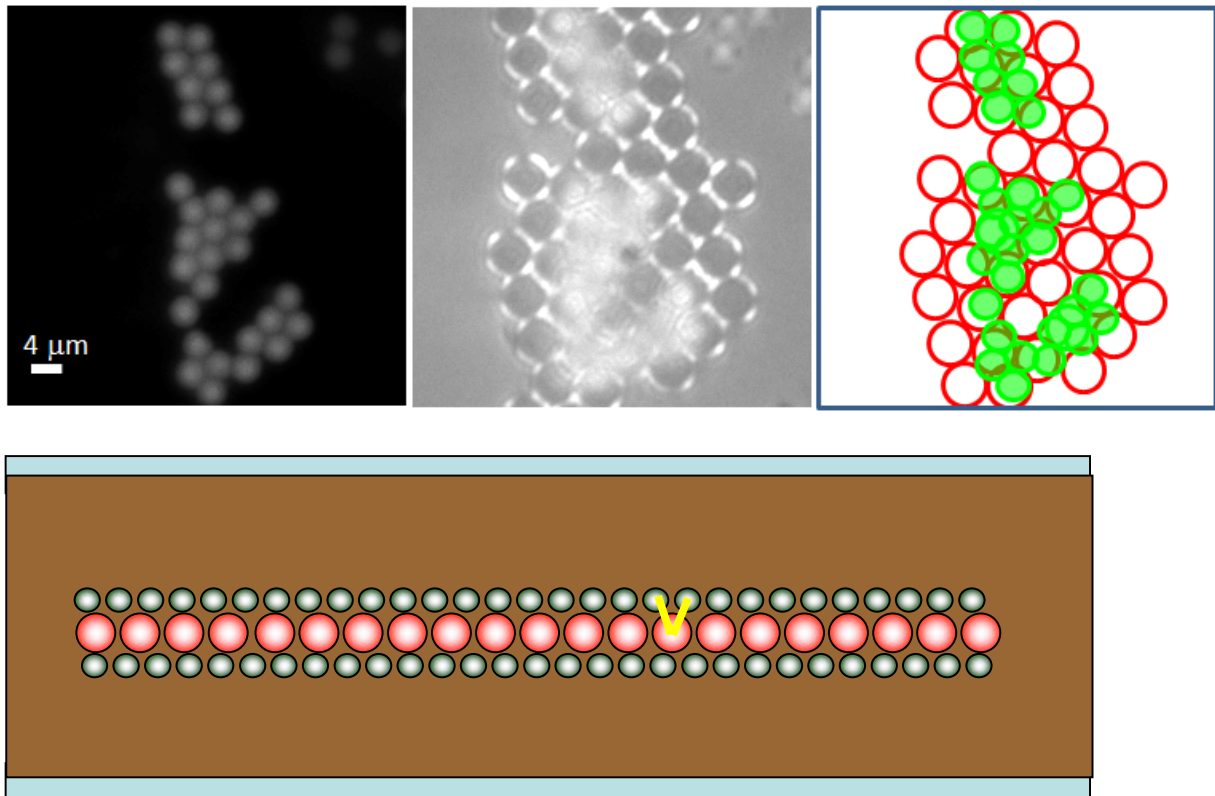


Figure 7: fluorescence- (top left), and polarization reflection microscope image (top middle) of an incommensurate crystalline phase $H_z=0\text{mT}$, $\Omega=120\text{s}^{-1}$, $H_{||}=1.82\text{mT}$, $2a_d=2.0\mu\text{m}$ (black). The top right picture shows a scheme of the packing of the paramagnets (red) and diamagnets (green). On the bottom we have a side view scheme of the incommensurate structure, where two paramagnetic diamagnetic bonds that are partially frustrated are shown in yellow.

We also observe the formation of disordered structures when neither the interdiamagnetic interaction nor the interaction of the diamagnets with the paramagnets dominates. Under such circumstances diamagnets may form small close packed incommensurate clusters on top of the perfectly ordered paramagnet that follow the periodicity of the paramagnetic lattice on a larger scale.

4 Discussion

The structure of the phases observed can all be understood by considering the time averaged dipolar interactions between the constituents (equation 7). Depending on the precession angle of the external field we expect paramagnets to bind to larger structures in bond angle directions that are attractive (violet in figure 2). In this way we obtain an assembly of paramagnets in the attractive bond directions $\varphi_b^{equi}, \mathcal{G}_b^{equi}$ that are all pointing with their magnetic moments in the same direction parallel to the external field. The order resembles a ferromagnetic ordering, however, the magnetic moments here are not permanent but are induced by the external field. We hence named the ordering an equimagnetic ordering. The time averaged dipole interaction between diamagnets behaves the same way creating a diamagnetic equimagnetic order with the diamagnetic moments all pointing antiparallel to the magnetic field. Bonds between diamagnets and paramagnets are attractive in bond directions $\varphi_b^{anti}, \mathcal{G}_b^{anti}$ perpendicular to the equimagnetic bond directions. In those orthogonal directions (orange bond directions in figure 2) we obtain an antimagnetic order of alternating para- and diamagnets that resembles a ferrimagnet, however, the alternating moments are induced moments not permanent moments.

The entire order hence consists of opposite magnetic particles that assemble in an alternating induced antimagnetic sequence in one or two directions while the arrangement is equimagnetic in the remaining directions. Whether the antimagnetic ordering is in plane and the equimagnetic is normal to the film or the other way round is controlled by the precession angle \mathcal{G}_{ext} of the external magnetic field. Antimagnetic equatorial ordering $\mathcal{G}_b^{anti} > \mathcal{G}_{magic}$ and equimagnetic polar $\mathcal{G}_b^{equi} < \mathcal{G}_{magic}$ ordering is supported by precession angles $\mathcal{G}_{ext} < \mathcal{G}_{magic}$ below the magic angle, while equimagnetic equatorial $\mathcal{G}_b^{equi} > \mathcal{G}_{magic}$ ordering and antimagnetic polar ordering $\mathcal{G}_b^{anti} < \mathcal{G}_{magic}$ is supported by angles $\mathcal{G}_{ext} > \mathcal{G}_{magic}$. It is for this reason colloidal flowers form at $\mathcal{G}_{ext} < \mathcal{G}_{magic}$ while sandwich structures are stable for $\mathcal{G}_{ext} > \mathcal{G}_{magic}$. When the precession angle of the magnetic field is

near magic $\mathcal{G}_{ext} \approx \mathcal{G}_{magic}$ we are in the regime where biaxial ordering prevails with equimagnetic ordering along one equatorial direction $\phi_b^{equi} = 0, \mathcal{G}_b^{equi} > \mathcal{G}_{magic}$ and antimagnetic ordering along $\phi_b^{anti} = \pi/2, \mathcal{G}_b^{anti} > \mathcal{G}_{magic}$ the other equatorial direction.

At large precession angles we observe the equatorial equimagnetic ordering with crystalline packing of the paramagnets and different types of packing of the diamagnets. The gaseous and different crystalline diamagnetic structures are controlled by the strength of thermal fluctuations and the dipole interactions. Whether the dipole interaction between paramagnets or diamagnets or between diamagnets and paramagnets dominates can be controlled via the susceptibility contrasts that can be changed by diluting the ferrofluid, the size of the particles, and the volume fraction of both types of particles. Small particles are mobile and prefer gaseous phases, large particles are immobile. At low volume fractions of diamagnets ϕ_d in a diluted ferrofluid ($\chi_F \ll 1$) their interaction with the paramagnets is stronger ($\propto \chi_F^1 \chi_p^1$) than the interaction between them ($\propto \chi_F^2$). Each paramagnet binds one diamagnet to its northpole leaving diamagnetic bonds frustrated because the diamagnets are separated more than their close-packed distance. It is for such conditions where we observe the enslaved crystal phase. In concentrated ferrofluid at a high fraction of diamagnets each paramagnet in the membrane can bind more than one diamagnet, the diamagnetic dipole interaction becomes stronger, such that diamagnets form a close packed membrane above the paramagnets as well. As a drawback some of the diamagnets reside at positions with bond angles to the paramagnet that are suboptimal (figure 7 bottom). In this limit paramagnetic diamagnetic bonds are partially frustrated and incommensurate phases are observed.

We can estimate the amount of neutralization between the paramagnets and diamagnets by the excess susceptibility

$$\Delta\chi_{eff} = \frac{M^{excess}}{H_{ext}} = [\Delta\chi_p \phi_p + \Delta\chi_d \phi_d] \quad (8)$$

, where ϕ_p , and ϕ_d are the volume fractions of para- and diamagnets. For our samples we had $\Delta\chi_{eff} > 0$ such that interactions between paramagnets dominate all other dipole

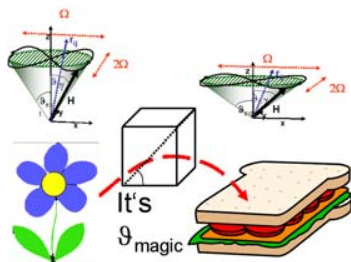
interactions. They hence formed structures they also would have formed without the presence of the diamagnets. The diamagnets, however, had to accept the distorted structure of the magnetic field, generated by the paramagnets and arrange themselves accordingly. Presumably when using truly neutralizing mixtures $\Delta\chi_{eff} \approx 0$, the then more symmetric situation between para- and diamagnets would produce even more interesting superstructures. At present we do not have ferrofluids of sufficient magnetic susceptibility to test such fully dipolar neutralized superstructures. However, even without having explored the full parameter space of possible structures it is clear that the control of the different parameters in the dipole interaction of different particles as well as the control of the volume fraction of particles allows the construction a rich variety of phases in a mixed diamagnetic and paramagnetic system.

5 Conclusions

Antimagnetically ordered colloidal phases with alternating arrangements of effectively diamagnetic and paramagnetic particles are formed in mixtures of paramagnetic and diamagnetic colloids immersed into a ferrofluid and subject to a quickly varying time dependent magnetic field. Depending on the mean orientation of the time averaged dyadic product of the external magnetic field the alternating order is observed in the plane of the film in form of colloidal flowers or normal to the film in the form of 2D paramagnetic crystals sandwiched between a diamagnetic gas or crystal. Near the magic angle eccentricity of the modulation creates also biaxial structures. The order of the diamagnetic sandwich layer depends on a subtle balance of parameters entering into the dipole interactions at work between the different particles

6 Acknowledgement

We thank Thomas Friedrich for helping with susceptibility measurements of the ferrofluids. This work is supported by the German Science Foundation within the cluster of excellence SFB840.



TOC-graph

7 References

- ¹ van Blaaderen, A.; Ruel, R.; Wiltzius, P.; *Template-directed colloidal crystallization*; *Nature* **1997**, 385, 321-324.
- ² Li, F.; Josephson, D. P.; and Stein, A.; *Colloidal Assembly: The Road from Particles to Colloidal Molecules and Crystals*, *Angew. Chem. Int. Ed.* **2011**, 50, 360 – 388.
- ³ Pieranski, P.; *colloidal crystals*, contemporary physics **1983**, 24 , 25-73.
- ⁴ Paunov, V. N.; Cayre, O. J.; *Supraparticles and "Janus" particles fabricated by replication of particle monolayers at liquid surfaces using a gel trapping technique*; *Adv. Mat.* **2004**, 16, 788-791.
- ⁵ Perro, A.; Reculosa, S.; Ravaine, S.; Bourgeat-Lami, E. B.; Duguet, E.; *Design and synthesis of Janus micro- and nanoparticles*, *J Mat. Chem.* **2005**, 15, 3745-3760.
- ⁶ Doye, J. P. K.; Louis, A. A.; Lin, I. C.; Allen, L. R.; Noya, E. G.; Wilber, A. W.; Kok, H. C.; Lyus, R.; *Controlling crystallization and its absence: proteins, colloids and patchy models*; *Phys. Chem. Chem. Phys.* **2007**, 9, 2197-2205.
- ⁷ Romano, F.; and Sciortino, F.; *Colloidal self-assembly: Patchy from the bottom up*, *Nature Materials* **2011**, 10, 171–173.
- ⁸ Sutera, S. P.; Boylan, C. W.; *nearly monodisperse population of prolate ellipsoidal particles useful for colloidal research*; *J. Colloid Interface Sci.* **1980**, 73, 295-297.
- ⁹ Nagy, M.; Keller, A.; *ellipsoidal polymer particles with predesigned axial-ratio* *Polym. Commun.* **1989**, 30, 130-132.
- ¹⁰ Glotzer S. C., and Solomon, M. J.; *Anisotropy of building blocks and their assembly into complex structures*; *Nature Materials* **2007**, 6, 557-562.
- ¹¹ Martin, J. E.; Venturini, E.; Gulley, G. L.; and Williamson, J.; *Using triaxial magnetic fields to create high susceptibility particle composites*; *Phys. Rev. E* **2004**, 69, 021508.
- ¹² Hynninen, A. P.; and Dijkstra, M.; *Phase diagram of dipolar hard and soft spheres: Manipulation of colloidal crystal structures by an external field*, *Phys. Rev. Lett.* **2005**, 94, 138303.
- ¹³ R. M. Erb, H. S. Son, B. Samanta, V.M. Rotello, B.B. Yellen, *Magnetic assembly of colloidal superstructures with multipole symmetry* *Nature* **2009**, **457**, 999-1002.

¹⁴ Osterman, N.; Poberaj, I.; Dobnikar, J.; Frenkel, D.; Ziherl, P.; and Babic, D.; *Field-Induced Self-Assembly of Suspended Colloidal Membranes* Phys. Rev. Lett. **2009**, 103, 228301.

¹⁵ A. Ray, S. Aliaskarsohi, and Th. M. Fischer; *Dynamics of self-assembly of flower-shaped magnetic colloidal clusters*; Phys. Rev. E **2010**, 82; 031406.

¹⁶ Ayan Ray, and Th. M. Fischer, *Core size effects on the rotation and stability of dipolar clusters in precessing magnetic fields*, Eur. Phys. J. E (in print)

Chapter 6

Summary

We have studied the effect of dipolar interactions on the statics and dynamics of mixed paramagnetic and diamagnetic colloidal particle system. In (chapter 3) We have studied magnetic dipole interactions in a self-assembled flower-shaped magnetic colloidal system. One of the question was how the diffusion in a dipolar interacting system differs from a short range interacting single file diffusion in a 1-dimensional system. We have measured the diffusion constant using Kubo's theory where we find out the mode dependency. We found that the response of the particles to conformational changes were less delayed in the dipolar system as compared with the hard-core single file diffusion systems. We have different modes of diffusion characterized by the Fourier index m and they decrease with the Fourier mode m while in the hard-core single file diffusion it increases. For m equals zero the diffusion constant of a hard-core system has the lowest value whereas, in our self-assembled flower-shaped magnetic colloidal cluster system we have the highest value. We have measured the angular velocity-autocorrelation functions where in the dipolar system we can see an instantaneous positive correlated response followed by an immediate

anti-correlate response. In a hard-core single file system the anticorrelated response follows after a significant delay. In a dipolar system, we have no separation of time scales because the long range nature of the dipolar interactions lets particle quickly react to changes in conformation that are far away from the particle.

In chapter 4, we have studied the order of the transition for the self-assembly of flower-shaped magnetic colloidal clusters and diamagnetic clusters in a precessing magnetic field. The transition is always first order but the strength of the first order transition is governed by the size of the core for both the clusters and the flowers. The order is strongly first order for large cores and weakly first order for small cores. We explain this by the deviation of the local magnetic field near the petals that is induced by the perturbation of the core.

In chapter 5, we have studied different ordering of paramagnets and diamagnets in a time dependent magnetic field. We have found three different motives of structures such as sandwiched membranes, strings, and flowers made from the composite mixture of paramagnetic and diamagnetic particles. In all structures bonds between similar particles form into directions orthogonal to directions of bonds between different particles.

In summary, we have shown, that long range anisotropic dipolar interactions between paramagnetic and diamagnetic colloids give rise to new static order, different forms of passive dynamics such as soft single file diffusion and to active non-critical dynamics. Both the long range and the anisotropy of the dipolar interactions lead to the emergence of new phenomena in colloidal systems.

Bibliography

- [1] HELGESEN, G. ; PIERANSKI, P. ; SKJELTORP, A. T.: Dynamic behavior of simple magnetic hole systems. In: *Phys. Rev. A* 42 (1990), 7271–7280. <http://dx.doi.org/10.1103/PhysRevA.42.7271>
- [2] LUTZ, Christoph ; KOLLMANN, Markus ; BECHINGER, Clemens: Single-File Diffusion of Colloids in One-Dimensional Channels. In: *Phys. Rev. Lett.* 93 (2004), Jul, 026001. <http://dx.doi.org/10.1103/PhysRevLett.93.026001>. – DOI 10.1103/PhysRevLett.93.026001
- [3] SKJELTORP, A. T.: One- and two-dimensional crystallization of magnetic holes. In: *Phys. Rev. Lett.* 51 (1983), 2306–2309. <http://dx.doi.org/10.1103/PhysRevLett.51.2306>
- [4] TIERNO, Pietro ; MURUGANATHAN, Ramanathan ; FISCHER, Thomas M.: Viscoelasticity of Dynamically Self-Assembled Paramagnetic Colloidal Clusters. In: *Phys. Rev. Lett.* 98 (2007), Jan, 028301. <http://dx.doi.org/10.1103/PhysRevLett.98.028301>. – DOI 10.1103/PhysRevLett.98.028301
- [5] WHITESIDES, G. M. ; GRZYBOWSKI, B.: Self-assembly at all scales. In: *Science* 295 (2002), 2418–2421. <http://dx.doi.org/10.1126/science.1070821>

-
- [6] XIA, Y. N. ; GATES, B. ; LI, Z. Y.: Self-assembly approaches to three-dimensional photonic crystals. In: *Adv. Mater.* 13 (2001), 409–413. [http://dx.doi.org/10.1002/1521-4095\(200103\)13:6<409::AID-ADMA409>3.0.CO;2-C](http://dx.doi.org/10.1002/1521-4095(200103)13:6<409::AID-ADMA409>3.0.CO;2-C)
- [7] ZERROUKI, D. ; BAUDRY, J. ; PINE, D. ; CHAIKIN, P. ; BIBETTE, J.: Chiral colloidal clusters. In: *Nature* 455 (2008), 380–382. <http://dx.doi.org/10.1038/nature07237>